Purinergic P2X receptors: structural and functional features depicted by X-ray and molecular modelling studies

Leanne Grimes and Mark T Young*

School of Biosciences, Cardiff University, Museum Avenue, Cardiff, CF10 3AX UK

*Corresponding Author; Email youngmt@cardiff.ac.uk

ABSTRACT
The publication of the first crystal structures of the zebrafish P2X4 receptor in 2009 was a pivotal moment; for the first time, researchers were able to interpret their experimental data in a structural context. Several research groups immediately set about using the data to make molecular models of the better-understood mammalian P2X receptors, in order to design and interpret the results of new, more focused structure-function experiments. In 2012, the publication of the crystal structure of zebrafish P2X4 in the ATP-bound state gave further insights into the mechanism of ligand binding and its coupling to ion channel activation, initiating a new cycle of modelling, experimentation and interpretation. The purpose of this review is to describe our current understanding of the 3D-structure of P2X receptors, by highlighting the strengths and limitations of the zebrafish P2X4 crystal structures, discussing how the molecular models derived from them have been made, and what they have been used for, and explaining why crystal structures of mammalian P2X receptors are still needed to uncover the molecular mechanisms of differential agonist/antagonist potency, allosteric modulation, pore dilatation and desensitisation.

KEYWORDS
P2X, structure-function, crystal structure, molecular modelling, molecular dynamics

RUNNING TITLE
Structure and molecular modelling of P2X receptors

1. INTRODUCTION

Since the cloning of the first P2X receptors in 1994 [1, 2], many elegant experiments have been performed using mutagenesis and functional assays to outline how these ion channels bind their ligand ATP, how ligand binding leads to channel opening, and how ions access and flow through the channel pore (summarised in [3]). A new era dawned in 2009, when the laboratory of Eric Gouaux published the first 3D-crystal structure of a P2X receptor, zebrafish (zf) P2X4.1 in the *apo*-, closed state [4], a towering achievement which was seven years in the making [5]. Now it was possible to visualise the architecture of the receptor and map the results from previous structure-function experiments, validating the structure as well as providing a structural context in which to interpret the data [6-8]. Furthermore, the availability of a crystal structure opened up new horizons; it was now possible to make molecular models of the well-studied mammalian P2X receptors and use them to design and interpret the results of new structure-function experiments. Much effort was expended upon using the closed-state structure to develop experiments to look at the conformational changes induced by ATP binding and the mechanism of ion flow [9-15]. This work provided some interesting insights into P2X receptor function; most notably the observation that ions flow into the P2X receptor transmembrane (TM) pore through lateral portals next to the extracellular face of the plasma membrane [12, 14, 15]. At this point it was clear that a 3D-structure of a P2X receptor in the ATP-bound state was required, and in 2012 the laboratory of Eric Gouaux provided one, presenting the crystal structure of zfP2X4.1 bound to ATP, in a conformation consistent with the open-channel state [16]. This structure confirmed the location of the ATP-binding site, identified the amino-acid residues involved in binding ATP, demonstrated that the lateral portals open in response to ATP binding, and showed a plausible mechanism for how the TM α-helices may move to open the ion channel. It opened up yet more possibilities for structure-based drug design, molecular modelling, and experiments to probe the mechanism of conformational changes induced by ATP binding [17-20].

In this review we will describe the key features of the zfP2X4.1 crystal structures, assess the implications of the mutations required to obtain well-diffracting crystals, and place zebrafish receptors in the context of the more widely studied mammalian P2X receptors, and other ligand-gated ion channels. We will also describe the published work on both low-resolution 3D-structures of P2X receptors, and homology models derived from the zfP2X4.1 crystal structures, and discuss how the models have been constructed and what they have been used for. Finally, we will outline why new structures of fully functional mammalian P2X receptors are essential, by stating what we still do not know about P2X receptor structure-function relationships, including the conformation of the intracellular domains, and the mechanisms of desensitisation and pore dilatation.

2. zfP2X4.1 CRYSTAL STRUCTURES

2.1 MOLECULAR PHARMACOLOGY OF zfP2X4.1 RECEPTORS

Nine P2X receptor genes have been identified in the zebrafish, *Danio rerio*, 6 of which are orthologs of mammalian P2X subtypes – *zfP2X1, zfP2X2, zfP2X3.1, zfP2X4.1, zfP2X5* and *zfP2X7*. Two of the other identified receptors correspond to *zfP2X3.1* and *zfP2X4.1* paralogs (*zfP2X3.2* and *zfP2X4.2* respectively), the final receptor has not been classified [21]. When comparing the full-length protein sequences, zfP2X4.1 protein displays significant sequence similarity to the mammalian P2X4 receptors, with an amino acid identity of 59% with rat (r) P2X4 and 58% with human (h) P2X4 (Sequence alignments – Supplementary Figure 1). Additionally, zfP2X4.1 is able to form functional homomeric channels, with properties comparable to the respective mammalian orthologs [22].

The zfP2X4.1 construct, which is 389 amino acids in length, contains many of the commonly conserved P2X domains identified in mammalian receptors. These include a cysteine-aspartate pair in TM2, 10 conserved cysteine residues in the extracellular domain, important for disulphide bond formation, and an N-terminal protein-kinase C motif [22].

When expressed in HEK cells, zfP2X4.1 channels display a similar electrophysiological and pharmacological profile to rP2X4 [23], exhibiting a slow, incomplete desensitisation in response to ATP, and little or no response to the ATP derivatives 2'(3')-O-(4-Benzoylbenzoyl) adenosine-5'-triphosphate (BzATP) and α,β-Methylene adenosine 5′-triphosphate (αβmeATP). Additionally, zfP2X4.1 is not inhibited by the non-selective P2X antagonists, pyridoxalphosphate-6-azophenyl-2',4'-disulfonic acid (PPADS) and suramin, which are also ineffective at mammalian P2X4 receptors [22, 24]. However, ATP is significantly less potent at zfP2X4.1 (EC_{50} = 275 – 800 μM [4, 22]) compared with the equivalent mammalian channels (rP2X4 EC_{50} = 10 μM [24, 25]; hP2X4 EC_{50} = 5.5 μM [26]).

2.2 ZEBRAFISH P2X4.1 CRYSTAL CONSTRUCTS – THE EFFECT OF MUTAGENESIS ON PROTEIN FUNCTION

zfP2X4.1 was chosen for structural studies following a screen of 35 different GFP-tagged P2X receptor homologs using fluorescence size exclusion chromatography (FSEC) following transient transfection in HEK-293 cells. The screen showed that zfP2X4.1 was capable of forming stable trimers in detergent and displayed a sharp, symmetrical elution profile following FSEC, which favoured it as a candidate for further structural studies. However, the addition of a GFP tag to zfP2X4.1 did affect receptor function; according to Kawate *et al*, the EC_{50} of ATP at wild type zfP2X4.1 was 800 μM, while the EC_{50} of ATP at zfP2X4.1-GFP was 1.73 mM [4].

To improve the crystallisation behaviour of zfP2X4.1, a number of modifications were made to the wild-type receptor. Firstly the N- and C-termini were truncated; 26 and 8 residue segments were removed from the N- and C-termini respectively to yield a crystal structure solved by single-wavelength anomalous diffraction in the presence of gadolinium (zfP2X4.1-A), which diffracted to 3.5 Å resolution (PDB ID 3I5D). Additionally, 3 further point mutations (C51F, N78K and N187R) were introduced to the extracellular domain to reduce both non-native disulphide bond formation and heterogeneity due to glycosylation (zfP2X4.1-B). The structure of zfP2X4.1-B was solved by molecular replacement, yielding crystals which diffracted to 3.1 Å resolution (PDB ID 3H9V). Although the mutated receptors were still responsive to ATP, the peak current amplitude was markedly reduced (by approximately 95% and 99% for zfP2X4.1-A and zfP2X4.1-B respectively) when compared to the wild type GFP-tagged channel. Additionally, the agonist sensitivity was markedly increased, with reported EC_{50} values of 27.4 μM and 3.4 μM for zfP2X4.1-A-GFP and zfP2X4.1-B-GFP respectively. Furthermore, the return of current to baseline on washout of agonist was significantly delayed in both crystal constructs [4]. These observations demonstrate that there are large differences in channel function between the wild-type and crystal constructs, and this must be borne in mind when interpreting structural data.

To solve the ATP bound structure of zfP2X4.1, additional mutagenesis of the receptor was required to improve crystallisation behaviour. Further truncation of the C-terminus (zfP2X4.1 final model, residues 36 – 359) and reversal of the initial C51F mutation gave rise to zfP2X4.1-C, which also displayed a sharp, symmetrical elution profile following FSEC. The zfP2X4.1-C structure was solved by molecular replacement, using zfP2X4.1-B as a search probe, at a resolution of 2.8 Å (PDB ID 4DW1; Figure 1B, D). Furthermore the structure of the *apo*-state zfP2X4.1-B construct was re-solved using new crystals which diffracted to a higher resolution of 2.9 Å (referred to as zfP2X4.1-B2; PDB ID 4DW0; Figure 1A, C) [16]. Electron density maps from new *apo*-state structure (PDB ID 4DW0) showed an incorrect assignment of electron density in the region encompassing residues 88 – 97 in the previously published structures (PDB IDs 3H9V and 3I5D). The functional properties of GFP-tagged zfP2X4.1-C were measured using two-electrode voltage clamp of *Xenopus* oocytes; the authors stated that the functional properties of this receptor were similar to that recorded for wild-type zfP2X4.1, yet their EC_{50} value was markedly different (2.1 μM compared to 1.73 mM for the wild-type GFP-tagged construct [16]). The authors did not report peak current values for wild-type zfP2X4.1 in their experiments, so it is not known how much peak current amplitudes were impaired by the introduced mutations, but it is clear from the current traces that zfP2X4.1-C also displayed delayed return of current to baseline values on washout of agonist, so from this evidence it is reasonable to assume that the function of zfP2X4.1-C was impaired in a similar fashion to the zfP2X4.1-A and zfP2X4.1-B crystal constructs. We argue that, while the crystal

structure derived from the zfP2X4.1-C construct clearly represents an ATP-bound structure, because of the impairment of function, it may well represent an artificially stabilised open state for the channel (because of the delayed return of current to baseline on washout of agonist).

2.3 HOW DOES zfP2X4.1 COMPARE TO THE MAMMALIAN P2X RECEPTORS?

zfP2X4.1 shares significant sequence similarity with mammalian P2X receptors. When comparing full-length protein sequences, it shares most amino-acid sequence identity with rP2X4 (59%) and least with hP2X1 (43%) (Supplementary Figure 1; sequence alignment).

2.3.1 ATP BINDING SITE

Preceding determination of the crystal structure of zfP2X4.1, mutagenesis and functional experiments were used to ascertain key residues involved in ATP binding of P2X receptors. P2X receptors do not contain any of the previously identified ATP binding motifs associated with other ATP binding proteins, such as the Walker motif [27]. It was hypothesized that polar and positive amino acids conserved across P2X subtypes may play a role in ATP binding and activity. Site-directed mutagenesis has been used to assess the function of some of these highly conserved residues at a number of P2X subtypes.

Residues thought to contribute to the ATP binding pocket have been identified in hP2X1, rP2X2, hP2X3 and rP2X4. Ennion *et al* studied the effect of mutating 11 conserved positive residues in the extracellular loop of hP2X1 [28]. K69A and K308A (rP2X2 numbering) mutations led to a dramatic reduction (< 1,400 fold) in ATP potency (as measured by EC_{50}). Even the conservative mutation K308R was 25-fold less sensitive to ATP. These results indicated that the individual chemical properties of the amino acid, as well as the charge, contribute to ATP binding. In addition, Lys-71 and Arg-290 were also proposed to contribute to the ATP binding pocket of hP2X1 [28]. Jiang *et al* performed an alanine-scanning mutagenesis study in rP2X2, identifying Lys-69, Lys-71 and Lys-308 as residues involved in ATP binding [29]. In this study, K69A and K308A mutations in rP2X2 gave rise to non-functional channels, and K71C mutant channels experienced a 1000-fold reduction in ATP potency [29]. In a separate study examining the ATP binding pocket of rP2X2, Leu-186 was shown to be involved in the binding of the adenine moiety of ATP [11]. Lys-69 and Lys-71 have also been implicated in agonist recognition in hP2X1, hP2X2, rP2X2, hP2X3, rP2X4 homomers and rP2X2/P2X4 heteromers [29-33]. Additional amino-acid residues implicated in agonist recognition are Lys-188 and Lys-308 (in hP2X1, hP2X2, rP2X2, hP2X3, rP2X4 and hP2X7 receptors) [28, 29, 31, 32, 34, 35] and Arg-290 (in hP2X1, rP2X2, hP2X3 and rP2X4 receptors) [28, 29, 36, 37].

Two separate studies indicate that ATP binds at the interface between 2 adjacent subunits, as opposed to within one subunit. The first study, by Wilkinson *et al*, used co-expression of mutant rP2X2 and rP2X3

subunits to demonstrate that the heteromeric P2X2/3 channel functioned normally when either Lys-69 or Lys-308 in the P2X2 subunit was mutated to alanine, but not when both lysines were mutated to alanine, or when wild-type P2X2 was co-expressed with a mutated P2X3 subunit. This showed that the heteromeric channel contained one P2X2 and two P2X3 subunits, that the receptor functioned essentially normally as long as two subunits were not mutated, and that Lys-69 and Lys-308 from two different subunits interacted in agonist binding [33]. The second study, by Marquez-Klaka *et al*, used a disulfide cross-linking approach in hP2X1, showing that mutation of Lys-69 and Phe-289 to cysteine led to both cross-linking between neighbouring subunits and a reduction in the size of currents elicited by ATP. Upon application of the reducing agent dithiothreitol (DTT), these currents were increased 60-fold, indicating an inter-subunit ATP binding site at hP2X1 receptors [38]. These results were later replicated with P2X2, but cross-linking between equivalent residues was less efficient in P2X3 and P2X4, indicating that one of these residues may not play a role in ATP binding in these subtypes [39].

In zfP2X4.1, the ATP binding site is embedded in the extracellular domain of the receptor at the interface between 2 subunits (with three such identical binding sites in the receptor trimer) (Figure 2A) [16]. The site is lined by a number of positively charged residues which form extensive hydrophilic interactions with ATP. ATP assumes a U-shaped conformation in the binding pocket; the phosphate groups form salt bridges and hydrogen bonds with surrounding polar and basic amino acids. In agreement with previous data, Lys-69 is shown to have a crucial role in ATP binding, forming critical interactions with all 3 phosphate groups. Additionally Asn-288 and Lys-308 form further contacts with the β-phosphate. The γ-phosphate further interacts with Lys-71, Arg-290 and Lys-308 residues (rP2X2 numbering) (Figure 2A) [16, 40].

The extensive number of interactions that the γ-phosphate forms with surrounding residues gives partial insight into why P2X receptors are responsive to ATP, but not to ADP or AMP [41]. However the β- and γ- phosphate groups are not fully submerged in the binding pocket, raising a possible explanation for the activation of rP2X receptors by diadenosine polyphosphates [42].

The adenine base is buried deep within the binding pocket and forms a number of interactions with highly conserved residues. The side chain of Thr-184 forms 3 hydrogen bonds with the adenine base. The adenine base also undergoes interactions with the carbonyl oxygen groups in the main chain of Lys-71 and Thr-184. Furthermore, hydrophobic interactions are formed with Leu-186 and Ile-226 (rP2X2 numbering) (Figure 2A) [16].

Many of the key residues identified in zfP2X4.1 as being involved in ATP binding are conserved across mammalian P2X receptors, and molecular modelling implies that a similar agonist binding site is likely to

exist in mammalian channels (see Figure 2B for a model of rP2X2 with bound ATP). Differences in the non-conserved residues lining the ATP binding cavity are likely to reflect subtype-specific differences in sensitivity to agonists and competitive antagonists. More detail on the key residues involved in ATP binding can be found in [18, 40].

2.3.2 PORE-LINING RESIDUES AND THE TM α-HELICES

Extensive mutational analysis has been used to study the TM pore-lining residues of P2X receptors. P2X receptors show differential preference towards certain cations, with rP2X2 displaying a higher affinity for calcium over sodium, for example [43, 44]. Additionally, rP2X2 receptors demonstrate a specific selectivity sequence to alkali metal cations [$K^+ > Rb^+ > Cs^+ > Na^+ > Li^+$]. This differs from the ions' relative mobility in water, indicating that the receptors are able to distinguish between cations, regardless of size, and that cations are likely to undergo weak interactions with the interior of the channel pore [45, 46].

The second TM helix (TM2) of rP2X2 contains a number of polar amino acids which are hypothesized to line the pore and form a hydrated surface for cation conductivity, regulating the current by solvating ions within the pore [47, 48]. Three of these polar residues in rP2X2 (Thr-336, Thr-339 and Ser-340) are thought to be important for cation selectivity. Mutation of Thr-336, Thr-339 or Ser-340 to the hydrophobic amino acid, tyrosine, led to a substantial change in calcium permeability and the alkali metal cation selectivity sequence (i.e. the receptor was no longer able to distinguish between the different ions). This data suggests the permeability sequence of rP2X2 is partly composed of these 3 polar amino acids in TM2 interacting with permeating cations [46].

In addition, mutation of Thr-339 in rP2X2 (T339S) gave rise to a channel with spontaneous activity. ATP was also ten times more potent at rP2X2 T339S compared to wild-type rP2X2, suggesting that the T339S mutation caused destabilisation of the closed channel. Lys-308 and Lys-69 are conserved residues, likely to be involved in ATP binding, as previously described. A K69A/T339S double mutant channel gave the same phenotype as the T339S single mutant. However a K308A/T339S mutant channel displayed no spontaneous activity, implying that Lys-308 may be involved in channel gating as well as ATP binding [49].

The crystal structure of zfP2X4.1 revealed that interactions between Leu-332, Leu-338 and Ile-347 are important for stabilizing the closed pore conformation. These interactions are broken upon activation of the channel as the TM helices move apart. Additionally, new interactions are formed between Leu-338 and Ile-347. The ion permeation pathway pore of zfP2X4.1 is lined by Leu-332, Ala-336, Ala-339, Leu-343 and Ile-347 (rP2X2 numbering). It is noteworthy that the majority of pore-lining residues possess

hydrophobic side chains. This is in contrast to the key residues hypothesized to line the mammalian P2X2 pore, which predominantly consist of polar amino acids. For example, in rP2X2, the equivalent amino acid to the hydrophobic isoleucine residue at position 347 is the polar residue tyrosine. This means that, in rP2X2, the polar side chains lining the pore may interact directly with the hydrated cations. These significant differences in pore lining residues imply there may be dissimilarities in the way cations pass through the TM helices in the zfP2X4.1 receptor and the mammalian receptors [16]. Clearly this observation has implications for interpretation of the pore function of mammalian P2X receptors based upon the zfP2X4.1 crystal structure.

2.3.3 THE N-TERMINAL DOMAIN

The roles of the N- and C-termini of P2X receptors in channel desensitization kinetics have been studied extensively in P2X1 and P2X2 receptors. The N-terminus of P2XRs contains a highly conserved protein kinase C binding site, TX(K/R). Two conserved N-terminal residues in rP2X2 (Thr-18 and Lys-20) are important for its slow rate of desensitisation compared to rP2X1. Abolition of the PKC consensus site via T18A, T18N and K20T mutations in rP2X2 gave rise to a change in channel kinetics, with channels undergoing fast desensitization in response to ATP. A P19A mutation gave rise to channels with similar desensitisation kinetics to wild type rP2X2 channels. These results demonstrate that the TX(K/R) PKC consensus site is a critical determinant of rP2X2 kinetics [50]. Similarly rP2X1 Y16C, T18C and R20C mutants experienced a reduction in peak current amplitude and changes in desensitization kinetics, demonstrating an important role for these residues in specific channel kinetics [51].

In 2013, Allsopp and colleagues used P2X1/2 N- and C- terminal chimeric proteins to investigate the effects of the intracellular termini on channel kinetics. They noted that mutating the N-terminal domain affected partial agonist efficacy (the magnitude of the maximal response), without altering agonist potency (no change in EC_{50}). Additionally, the first 16 amino acids of the N-terminus predominantly control agonist efficacy, whereas the N-terminal region adjacent to TM1 is likely to fine-tune these effects [52]. Specifically, residues 21-23 were suggested to affect desensitization in P2X1 and P2X2 receptors. [53].

The zfP2X4.1 construct used for crystallization contained an N-terminal truncation (28 amino acids), therefore all the residues identified above with roles in channel kinetics of P2X1 and P2X2 were removed prior to protein expression, purification and structure determination. This N-terminal truncation may therefore account for the large reduction in peak amplitude in response to ATP observed for the zfP2X4.1 crystal constructs. It may also play a role in delayed return of current to baseline after washout of agonist.

2.3.4 THE C-TERMINAL DOMAIN

The C-terminal domains of P2X receptors display high amino-acid sequence variability; furthermore, P2X2 and P2X7 receptors have long intracellular C-termini (approximately 110 and 250 amino-acids in length respectively) for which no structural information is available. Despite their variability, these domains are thought to play important roles in channel kinetics, in particular in agonist sensitivity and recovery from desensitization. Partial agonists which displayed high efficacy at P2X1 receptors, and low efficacy at P2X2 receptors, displayed intermediate efficacy at a P2X1-2C chimera. In addition, the C-terminal domain was associated with a decrease in agonist potency. Furthermore, residues 360-364 of the C-terminal domain were shown to be involved in the regulation of channel recovery from desensitisation [52].

Additional potential PKC sites are present in the C-terminus of rP2X2 at Thr-372 and Thr-464. Elimination of these sites from rP2X2 via a truncation of the receptor at His-375 and mutation of Thr-372 gave rise to channels which displayed rapid desensitisation. Additionally, truncated channels in combination with N-terminal PKC site mutations (T18A, K20T) displayed peak currents with a significantly smaller amplitude. This data indicates that in addition to the PKC site in the N-terminus, P2X2 receptors require specific intracellular interactions between the 2 cytoplasmic domains for complete cell surface expression of slowly desensitising channels [50].

The C-terminal domain of all P2X receptors contains a YXXXK motif 8-18 residues downstream of TM2 which is involved in plasma membrane targeting of the receptors. Mutation of any of these residues in rat P2X2 resulted in decreased cell surface expression [54]. The C-terminal domain of zfP2X4.1 was truncated at position 359 in zfP2X4.1-C; therefore the YXXXK trafficking motif is absent and this may have a significant effect on receptor function (lower peak currents resulting from fewer receptors at the cell surface).

Additionally mammalian P2X4 receptors contain a tyrosine based, endocytic motif (YEQGL). Mutation of the tyrosine residue leads to a reduction in the rate of receptor internalisation [55]. Although this motif is not present in zfP2X4.1, the equivalent residues following the tyrosine (GLLH) are truncated in the zfP2X4.1 construct used for crystallisation. Therefore if wild type zfP2X4 undergoes rapid internalisation and reinsertion into the membrane, disruption of these residues may have an effect on channel trafficking and function.

2.4 *APO- VERSUS* ATP-BOUND CRYSTAL STRUCTURES

Publication of the crystal structures of the *apo-* and ATP-bound states of zfP2X4.1 receptors has provided valuable insight into the structure and mechanism of action of P2X receptors. The structures have enabled

us to identify key residues involved in agonist binding and pore-lining residues with roles in cation selectivity [4, 16].

Kawate *et al* liken the receptor monomer to a leaping dolphin and the various domains have been named accordingly (Figure 3A). The TM helices are referred to as the tail or fluke of the dolphin. The extracellular domain is made up of the upper body, lower body, dorsal fin, the left and right flippers and the head region. The body region of the dolphin is made up of β-sheets to form a β sandwich structure. Three monomers wrap round one another to make the trimer (functional unit) (Figure 1A). The majority of subunit-subunit interactions are formed in the upper body domain, with fewer interactions formed in the lower body domain, proximal to the TM helices, which is consistent with a structure that permits movement (transmission of a conformational change induced by agonist binding to the channel pore) [16].

Mammalian P2X receptors contain 10 extracellular, conserved cysteine residues which form 5 disulfide bond pairs; 1-6 (Cys-119-Cys-168), 2-4 (Cys-129-Cys-152), 3-5 (Cys-135-Cys-162), 7-8 (Cys-220-Cys-230), and 9-10 (Cys-264-Cys-273). Using rP2X2 numbering this corresponds to 1-6 (Cys-113-Cys-164), 2-4 (Cys-124-Cys-147), 3-5 (Cys-130-Cys-158), 7-8 (Cys-214-Cys-224) and 9-10 (Cys-258-Cys-267). These disulfide pairings are confirmed by the zfP2X4.1 crystal structure (Figure 3B, C) [4]. Disulfide pairs 1-6, 2-4 and 3-5 are located in the head region of the receptor (Figure 3B), 7-8 is situated in the dorsal fin region and 9-10 in the lower body region (Figure 3C) [4]. Disulfide bonds have important roles in the formation and maintenance of ion channel structure. In hP2X1 receptors, although all single cysteine residue mutants gave rise to functional channels, some of the mutants (C264A, C273A, C135A, C162A corresponding to the 3-5 and 9-10 disulfide bond pairs (zfP2X4.1 numbering)) caused a reduction in current amplitudes. Additionally C264A and C273A channels are not efficiently trafficked to the cell surface. These results indicate that Cys-264 and Cys-273 are involved in the formation of a disulfide bond and disruption has implications on the tertiary structure of the protein, thereby preventing it from being trafficked to the cell membrane [56]. Although the conserved disulfide bonds are clearly important in mammalian P2X receptors, it should be noted that *Dictyostelium discoideum* P2XA (DdP2XA) does not contain any of them (according to sequence alignment); however, DdP2XA is still functional, and low-resolution structural studies indicate that it has a similar architecture to zfP2X4.1 [57].

The extracellular domain of zfP2X4.1 appears to be shaped like an equilateral triangle (Figure 1C), extending approximately 70 Å above the membrane. The TM-spanning region is 28 Å long; the helices show a left-handed twist orientation and are anti-parallel to one another, approximately 45° from the membrane plane [4]. The TM pore is predominantly lined by the TM2 helices, with the TM1 helices

positioned peripherally. In the *apo*-state, the TM pore is occluded by the sidechains of Leu-340 and Ala-347 (Ile-332 and Thr-339 in rP2X2). In the ATP-bound state, the pore is open and continuous; the diameter at the narrowest point (bounded by the sidechains of Ala-347 and Leu-351 (Thr-339 and Val-343 in rP2X2)) is approximately 7Å [16].

Superposition modelling of the two channel states shows that ATP binding does not greatly affect the conformation of the upper body domain, inferring that this part of the structure stays relatively rigid upon activation. Conversely, the lower body domain undergoes substantial conformational changes upon agonist binding, resulting in an outward 'flexing' of the lower body domain (Figure 1B). Movement of these domains results in an expansion of the TM helices [16]. The TM helices undergo conformational changes in an iris-like movement when ATP binds to the extracellular domain. TM1 and TM2 rotate anticlockwise by 10° and 55° respectively proximal to an axis perpendicular to the membrane plane. Their tilt angle is also increased by 8° and 2° respectively about an axis parallel to the membrane. These movements result in the helices moving away from the central axis, allowing expansion of the ion conducting pore to a width which would permit the flow of ions through the channel, consistent with a transition from closed- to open-state.

Inspection of the electron density of both the *apo*- and ATP-bound states reveals that it is of poorest quality in the TM regions, which is not unusual for membrane proteins. Several side chain positions within the TM helices cannot be assigned, and so care must be taken when interpreting data for the TM helices with these structures. This is additionally important because of the truncation of the N-terminal domain and its potential effect on channel properties. It might be possible to resolve these issues by obtaining structures of the *apo*- and ATP-bound states in membrane environments rather than detergent micelles, but it is worth noting that, for the transporter LeuT, crystal structures of different conformational states of the protein in detergent micelles and lipid bicelles were virtually identical [58].

Lateral fenestrations present in the extracellular vestibule of the receptor open wide upon ATP binding and provide a pathway for the influx of cations into the channel (Figure 1B). Once the ions have entered through the fenestrations, the highly acidic residues of the central vestibule attract only cations and repel anions, which is thought to contribute to the cation selectivity of the channel [12, 15, 16, 59, 60].

The structure determination of zfP2X4.1 represents the first major breakthrough in high-resolution imaging of a P2X receptor, providing great insight into the mechanism of action of the receptor. However, as noted above, zfP2X4.1 displays markedly different characteristics to most mammalian P2X receptors (relatively low ATP potency, hydrophobic residues lining the channel pore), and the function of the crystal constructs was significantly different to wild-type zfP2X4.1, meaning that a degree of caution

must be exercised when either interpreting functional data for mammalian P2X receptors using the zfP2X4.1 structures, or using the structures as templates for molecular modelling. With this in mind it is still important to strive for high-resolution structures of mammalian P2X receptors, both for comparative structural biology and structure-based drug design.

2.5 SIMILARITY TO ACID-SENDING ION CHANNELS (ASIC)

Acid sensing ion channels (ASICs) are cation-selective ligand-gated ion channels activated by protons which can exist in a desensitized, closed state or an open state under low or high pH conditions. In 2009 the structure of chicken ASIC1 was solved in the desensitized state, which revealed some common architectural similarities with P2XRs (compare Figures 4A and 4B) [61]. The crystal structure showed that ASICs are also trimeric with each subunit composed of two TM helices, a large cysteine-rich extracellular domain and intracellular N- and C- termini. Despite the clear structural similarities and common functional properties between P2XRs and ASICs, these two classes of channels do not share any obvious significant sequence similarity [4, 62].

The TM helices of ASICs and P2XRs are very similar in structure. The first crystal structure of chicken ASIC1 was published in 2007 at 1.9 Å resolution [62]. However this structure was a non-functional mutant and the TM regions were later rectified upon publication of the structure of a functional channel in 2009 at 3 Å resolution [61]. The crystal structures of ASIC1 and zfP2X4.1 revealed that both the TM pores are lined by the TM2 helices, with the TM1 helices located peripheral to TM2 (compare Figures 4C and 4D). Superposition modelling of the TM2 helices alone showed them to be approximately equivalent in both receptors [61].

Following superposition modelling of these two channels, sequence alignments of the TM2 helices revealed new, unforeseen sequence similarities. For example Asp-Ile-Gly and Asn-Ile-Gly motifs were identified at the base of the extracellular vestibule in ASIC1 and zfP2X4.1 respectively; the aspartate and asparagine (residue 338 in zfP2X4.1) residues are both essential for ion channel function [63, 64]. The gates of both channels are formed from the crossing of TM2 helices with Gly-436 and Ala-344 representing these crossing points in ASIC1 and zfP2X4.1 respectively. The gates are made up of 5-8 adjacent amino acids [61]. However there are also some key differences between the TM structures. Leu-340 in zfP2X4.1 corresponds to Gly-432 in ASIC1, this is known as the degenerin position in ASICs. Mutation of this residue to larger amino acids in ASIC1 leads to constitutive channel activation [65]. However this is not the case with zfP2X4.1, with a neighboring proline residue, one helix turn upstream of Leu-340, bending the helix and likely making space for this large side chain [61].

The vestibule domains of ASIC1 and zfP2X4.1 are also remarkably similar. Both channels consist of an 'upper' vestibule, a 'central' vestibule, an 'extracellular' vestibule (lateral portal) which is located proximal to the pore, and the 'cytoplasmic' vestibule. The central and extracellular vestibules are lined by acidic residues, making them highly electronegative. This feature contributes to the cation selectivity of both channels. The central vestibule of zfP2X4.1 is accessible in the closed state structure. Although the vestibule is not accessible in the desensitized ASIC1 structure, previous data has shown that the central vestibule is accessible in the resting state of ASIC3 accordingly [61, 66]. Crystallization of the ATP-bound, open state zfP2X4.1 and psalmotoxin (PcTx1 – a selective gating modifier) bound, open state ASIC1 has revealed that ions enter both channel pores via lateral fenestrations and cannot travel through the central vestibule (Figure 4B) [16, 67].

Although the extracellular domains of ASICs and P2XRs are largely different due to the differential agonist binding (i.e. ATP at P2XRs and protons at ASICs), the core of the extracellular domain is similar; the TM helices are connected to β-strands which make up part of a large β-sheet. Structural elements involved in ligand binding and conformational changes surround this central β-sheet core in both channel types [68].

Crystallization of the open state structures has enabled identification of the ligand binding sites in P2XRs and ASICs. As previously described, P2XRs contain 3 inter-subunit ATP binding sites, approximately 40 Å from the membrane plane [16]. ASICs contain 3 equivalent PcTx1 binding sites at the subunit interfaces, located approximately 50 Å from the membrane plane [67].

A comparison of the closed, desensitized ASIC1 channel with the toxin-bound, open-state structure under low and high pH conditions revealed that very similar conformational changes occur in ASIC1 upon agonist binding, compared with what is observed for P2X receptors. The upper part of the extracellular domain remains relatively rigid and immobile upon activation, whereas the lower parts of the extracellular domain are more flexible, and expansion of the β-strands in this region leads to expansion of the extracellular vestibule, resulting in a conformational change in the TM region and channel opening. However, the conformational changes occurring in the TM helices themselves are significantly different from those that occur in zfP2X4.1 [68, 69].

3. OTHER DIRECT STRUCTURAL DATA FOR P2X RECEPTORS

Although the crystal structures of zfP2X4.1 in the *apo*- and ATP-bound state represent our only high-resolution structural data for P2X receptors, a number of other direct structural studies of P2X receptors have been carried out, using either atomic force microscopy (AFM) [70-74] or transmission electron microscopy (TEM) [14, 57, 75-77]. While these studies have produced data of significantly lower

resolution compared to the crystal structures, they are still useful because (i) they give estimates of the overall size and shape of P2X receptors, and (ii) some studies have been carried out in the absence and presence of ATP in an attempt to image conformational changes induced by ligand binding. These data can be compared with that derived from the zfP2X4.1 crystal structures for cross-validation – to what extent do the low-resolution and high-resolution studies agree?

3.1 AFM IMAGING

AFM is a technique that produces structural data by scanning over the surface of a specimen with a fine tip. The resulting images represent a topographical map of the specimen and can give information about both sample thickness and shape changes in response to a stimulus. AFM was first used on P2X receptors to analyse oligomer formation in rP2X2 and P2X6 expressed in human cells [72]. In this elegant study, the authors demonstrated, by measuring a mean angle between bound antibodies of 123°, that rP2X2 receptors formed trimers with a mean volume of 409 nm^3, or 1.7nm^3/kDa, which agrees well with a value of 1.2 nm^3/kDa calculated for the zfP2X4.1 crystal structure [8]. The authors also demonstrated that P2X6 receptors were unable to form homomeric trimers, but later demonstrated that P2X2/6 heterotrimers could form in different stoichiometries, which were solely dependent on relative protein concentration [71]. The same group have since developed general methods to analyse the subunit stoichiometry of a range of different ligand-gated ion channels [70]. Another early AFM study utilised rP2X2 receptors purified from over-expression in insect cells [73]. This study imaged particles of approximately 10 nm in the presence of ATP, detecting the presence of a central depression which the authors interpreted as evidence for the appearance of a pore in the protein. Although the size of the particles is broadly consistent with that of zfP2X4.1, the observation of a central depression is quite surprising considering that in the zfP2X4.1 open-state crystal structure, the route of ion entry appears to be *via* lateral portals [16]. However, P2X2 has a long intracellular domain, and we know little about its structure; it might be possible that Nakazawa *et al* observed a conformational change in the intracellular region of the protein induced by ATP binding. Fast-scanning AFM accompanied with single-particle averaging techniques has been used to image rP2X4 receptors in the absence and presence of 1 mM ATP on a polylysine-coated mica substrate [74]. In the absence of ATP, rP2X4 appeared as rounded triangles with a mean diameter of 12.6 nm, consistent with the shape and dimensions of the zfP2X4.1 crystal structures. Surprisingly, ATP treatment caused significant structural changes; the rounded triangle separated into three discrete circular densities, which the authors interpreted as consistent with each subunit of the trimer moving away from a central pore as the channel opened. This interpretation is not consistent with the conformational changes observed in the ATP-bound zfP2X4.1 crystal structure [16], where the subunits remain in close contact with each other. One puzzling observation from the AFM data was that the mean particle height was <4 nm, which is significantly shorter than the length of the zfP2X4.1 crystal structure (approximately 10 nm [78]). The

same thickness was observed even when the channels were imaged in lipid bilayers, and may have resulted from the particles being significantly tilted to the side, or twisted [74]. It is plausible to speculate that, if imaged on their side, the opening of lateral portals in P2X receptors in response to ATP binding might appear as a separation of subunits, but it is also important to note that while particles on their side would not possess 3-fold symmetry, particle averaging using forced 3-fold symmetry would still give the impression of 3 subunits separating.

3.2 TEM AND SINGLE PARTICLE ANALYSIS (SPA)

Generating 3D-structures of purified membrane proteins using TEM and SPA has two significant advantages over X-ray crystallography. First, a much lower protein concentration is required (50-100 μg/ml for imaging in negative-stain and 0.5-1 mg/ml for imaging under cryo-conditions, compared to approximately 10 mg/ml for 3D-crystallography). Second, the protein may be imaged in its native state, and there are no potential artefacts induced by crystallisation. The significant disadvantage of the technique is that the obtainable resolution is usually much lower. In negative-stain imaging, the resolution is limited to approximately 20 Å, and the stain does not penetrate the detergent micelle that surrounds the TM helices. Imaging under cryo-conditions, where the ice surrounding the specimen is frozen so rapidly that it vitrifies, avoiding sample damage by ice crystal formation, provides the highest resolution, but due to technical limitations, the practical lower limit of molecular mass for a protein to be imaged successfully using cryo-EM is approximately 200 kDa [79]. However, for symmetrical proteins larger than this, using direct electron detection and image stabilisation algorithms, it is now possible to obtain data of high enough resolution to solve membrane protein structures (3.5 Å), as illustrated by the recent publications of structures of TRPV1 (the modified 'minimal functional construct' used was a tetramer of approximately 270 kDa in mass) in native and ligand-bound states [80, 81]. It is worth noting that significant optimisation of the construct by mutagenesis was required to generate protein of sufficient homogeneity to achieve high resolution, but it is also of note that the final protein concentration required was only 0.7 mg/ml. This spectacular advance hints at the significant potential of cryo-EM and SPA for membrane protein structural studies, and it is likely that the technique will improve further in the future to allow the study of smaller proteins, including the P2X receptors.

A number of P2X receptors have been imaged using TEM and SPA to produce 3D-structures. The first to be imaged was rP2X2 in negative-stain, purified from over-expression in insect cells [75]. In this study the authors were unable to produce a 3D-structure due to uneven staining, but stated that the extracellular domain had a crown-capped structure, with an estimated volume derived from its dimensions of approximately 1200 nm^3 (equating to 5 nm^3/kDa, much larger than that reported for rP2X2 by AFM or the zfP2X4.1 crystal structure (see above). The same group went on to image rP2X2 under cryo-

conditions [76], obtaining a 3D-structure at a resolution of 22 Å (FSC=0.5 criterion; Figure 5A). Subsequently, 3D-structures have been obtained using TEM of negatively-stained protein for hP2X4 [77] (Figure 5B), *Dictyostelium discoideum* P2XA (DdP2XA) [57] (Figure 5C) and hP2X1 in the absence (Figure 5D) and presence (Figure 5E) of 1 mM ATP [14]. Each structure is displayed at approximately the same scale in Figure 5; it is clear to see that the rP2X2 structure is significantly larger, and also displays more cavities than the other structures. DdP2XA has been fitted with the crystal structure of zfP2X4.1 for comparison (Figure 5C); this demonstrates that the overall dimensions of the low-resolution hP2X4, DdP2XA and hP2X1 structures are comparable with those of zfP2X4.1. Figure 5D and 5E demonstrate that, even at low resolution, elements of the conformational change induced by ATP (contraction of the head region and opening of lateral cavities) may be observed [14]. In our opinion, the large discrepancy observed between the dimensions of the rP2X2 cryo-EM structure and the zfP2X4.1 crystal structure serves to highlight the technical challenges of using cryo-EM imaging on proteins at or slightly below the 200 kDa cut-off (P2X2 trimers are approximately 180 kDa), and it is plausible that, in the cryo-EM experiments, small heterogeneous protein aggregates were imaged rather than receptor trimers (these aggregates have been observed previously for rP2X4 [4]).

4. MOLECULAR MODELLING OF P2X RECEPTORS

Since the publication of the crystal structure of zfP2X4.1, a number of researchers have generated homology models of P2X receptors (mostly the mammalian receptors for which the pharmacology and function is best-understood) in order to either map or design point mutations for structure-function studies. The accuracy of homology modelling largely depends on the quality of the sequence alignment between the template and target sequence; when the sequence identity is high (>70%), modelling is likely to be successful, but when it is low (<30%), the models generally fail to improve on the starting structures [82]. For membrane proteins, it is possible to construct acceptable models of the TM domains for template sequence identities of 30% or higher (provided that the sequence alignment is good), but the alignments in the soluble regions are likely to be less accurate [83]. Amino-acid sequence identity between the region of zfP2X4.1 included in the crystal structures and the human P2X receptors varies from 45% (hP2X6) to 62% (hP2X4), which is intermediate between the zones of high and low confidence in model accuracy. The fact that the models may not be particularly accurate representations must be borne in mind when using them to map and design mutations. The published molecular models, along with how they were generated, and what they have been used for, are listed below by receptor subtype. A further point of note is that the crystal structures of zfP2X4.1 were all determined from protein where the hydrophobic TM helices were stabilised using detergent micelles. It is often useful when modelling to be able to estimate the probable orientation of the protein within the lipid bilayer (in terms of its tilt angle and the bilayer thickness next to the protein). The Orientations of Proteins in Membranes (OPM) database

(http://opm.phar.umich.edu/) provides spatial arrangements of membrane proteins in the lipid bilayer. Each protein is positioned in a lipid bilayer of adjustable thickness by minimizing its transfer energy from water to the membrane [84]. OPM have estimated the position of the membrane around PDB IDs 3H9V and 4DW1 and these models are freely available to download.

4.1 P2X1

A homology model of hP2X1 was constructed using the trimeric zfP2X4.1 structure at 3.5 Å resolution (PDB ID: 3I5D) [14]. The authors used Modeller software [85] to construct the initial model, then WHAT-CHECK [86] and ProSA-web [87] to assess model quality. This model was then used to map the change in accessibility of a series of cysteine mutants from Glu-52 to Gly-96 (extracellular end of TM1, through regions of the extracellular domain lining the lateral portals and internal vestibules) in the absence and presence of ATP, finding that ATP binding induced contraction of the internal vestibules without altering access to the lateral portals. The same model and set of mutants was later used to analyse agonist binding and channel gating [30]; in this work both ATP and BzATP were docked into the model using GOLD [88], allowing comparison of the docking with experimental data. A third publication using the model analysed the effect of deletion and mutation of the head region of P2X1 on channel function, suramin and NF449 sensitivity [89]. Lorinczi *et al* constructed a homology model of rP2X1 using Modeller, using it to map the conformational changes in the head region of the receptor using cysteine mutagenesis, tetramethyl rhodamine maleimide (TMRM) labelling and voltage-clamp fluorometry [90]. They found that movements of the head domain were involved in both activation and desensitisation of rP2X1, and also used Autodock Vina software [90] to dock both ATP and TMRM into their model to interpret their experimental data.

4.2 P2X2

P2X2 is probably the best-understood member of the P2X receptor family, in terms of mutagenesis and structure-function studies. Therefore it is not surprising that it has been modelled the most times. Initial studies used models of rP2X2 to map amino-acid residues important for gating, conductance and rectification, either using PDB ID 3H9V (zfP2X4.1 at 3.1 Å resolution) [91] and Modeller, or PDB ID 3I5D [92] and the SWISS-MODEL server [93, 94]. Modeller was also used in three further studies; the first of which analysed the subunit interfaces, providing evidence for the formation of an intracellular salt bridge between Glu-63 and Arg-274 important for rP2X2 channel function [95]. The second study used cysteine mutants in the putative ATP binding site and a thiol-reactive ATP analogue (NCS-ATP) to trap ATP in the binding site using crosslinking [11]. The authors found evidence for two distinct modes of ATP binding, and were able to produce NCS-ATP-docked models of rP2X2 using Autodock Vina. The third study looked at cysteine accessibility and disulphide bridge formation in cysteine mutants of rP2X2,

demonstrating that ions preferentially flow into the TM helices *via* lateral portals rather than through the central portion of the extracellular domain [12].

In other studies, further validation was performed to produce models useful for the interpretation of mutagenesis data on the permeation of ions through the channel pore; Kracun *et al* used PDB ID 3H9V and Modeller, then inspected their model using Coot [96], and refined it using maximum likelihood methods with REFMAC [97]. Their data identified, using the substituted cysteine accessibility method, the accessible amino-acid residues in the P2X2 pore and demonstrated that the narrowest part of the pore was consistent with that observed in the zfP2X4.1 crystal structure [59]. Browne *et al* used Modeller and Coot as above, but assessed model quality using the MolProbity server [98], and performed energy minimisation using UCSF Chimera [99]. Their data demonstrated that the closed-to-open transition of rP2X2 required a symmetrical separation of the three subunits in the trimer [9]. Molecular Operating Environment Software (MOE2008.10) has also been used to model rP2X2 using PDB ID 3H9V as a template, docking in suramin derivatives, including NF770, which demonstrates that, in the closed-state structure, the binding pocket is large enough to accommodate an entire NF770 molecule [100]. Punthambaker *et al* modelled hP2X2 using PDB ID 3H9V, SWISS-MODEL and Coot, using it to identify a cluster of three histidine residues forming a region with the potential to control the mode of zinc inhibition (His-204 and His-209 in one subunit, and His-330 in an adjacent subunit) [101]. They found that mutation of all three histidine residues decreased the potency of zinc inhibition by 100-fold, showing that the histidine cluster controlled the access of zinc to its binding site.

Three recent studies have made use of both *apo*- and ATP-bound molecular models of rP2X2, using PDB IDs 4DW0 (the new, corrected *apo*-state structure at 2.9 Å resolution) and 4DW1 (the ATP-bound structure at 2.8 Å resolution), Modeller, Molprobity and UCSF Chimera. These studies have employed disulphide locking to probe movements in the extracellular domain of the receptor induced by ATP binding [102], lipophilic attachment at the top of TM2 to induce direct channel gating [103] (also see Section 4.7) and cysteine mutagenesis coupled by attachment of thiol-reactive azobenzene crosslinkers to make rP2X2 receptors sensitive to light [104]. A separate study by Lemoine *et al* also made use of azobenzene crosslinkers to induce optical gating in rP2X2 [105], using molecular models generated from PDB IDs 4DW0 and 4DW1 with Modeller and Autodock. These studies demonstrate the power of using molecular modelling using different channel states to design experiments to understand the conformational changes induced by channel opening, and to generate P2X receptors with novel and useful additional features.

4.3 P2X3

A homology model of P2X3, constructed using Modeller and validated using Procheck [106] has been used to investigate the contribution of the conserved TM1 residue Tyr-37 to the rapid desensitisation observed in this receptor subtype [107], and the contribution of Ser-275 in the left flipper region of the receptor to closure of the ATP-binding pocket after ATP binding [108]. Both studies required the molecular models to enable experimental design. Riedel *et al* made a model of rP2X3 using Modeller, and then used Autodock Vina to dock ATP and its analogues into the binding site [109]. On superficial inspection ATP does not appear to adopt the U-shaped conformation seen in the crystal structure of zfP2X4.1 with ATP bound [16], but as previously observed, there is some evidence that ATP may be able to bind to P2X receptors in more than one conformation [11]. Li *et al* made models of rP2X3 using PDB IDs 3H9V and 4DW1 and SWISS-MODEL to investigate the inhibitory effect of magnesium at P2X3 receptors. They demonstrated that free ATP (ATP^{4-}) was able to activate all mammalian P2X receptors capable of forming homotrimers, and furthermore that the inhibitory effect of magnesium was *via* binding to a central cavity in the extracellular domain [110].

4.4 P2X4

Given that hP2X4 is most similar to zfP2X4.1 (62% identity in the region described by the crystal structure), and should therefore produce the most accurate molecular model, it is perhaps surprising that more studies have not used it to interpret structure-function data. One major study used a model of hP2X4 made using PDB IDs 3H9V and 3I5D and SWISS-MODEL to demonstrate that labelling cysteine mutants lining the lateral portals of the receptor (Glu-56 and Asp-58) with 2-(trimethylammonium)ethyl methane thiosulfonate (MTSET) significantly reduced the amplitude of currents elicited by ATP [15]. This data confirmed the preferential use by ions of the lateral portals just above the TM helices. Another study generated a model of hP2X4 derived from PDB ID 3H9V using Modeller and validated using Molprobity and Chimera to map the positions of residues shown to be modified with N-linked glycans, demonstrating that each was surface-accessible in the molecular model [57].

4.5 P2X7

Three studies have been published which use a molecular model of hP2X7 based upon PDB IDs 3H9V and 3I5D, and built using Modeller, Molprobity and Modloop [111] (to model the non-conserved region of P2X7 between the β2 and β3 strands, approximating to residues 72-84 of hP2X7). Roger *et al* mapped single nucleotide polymorphisms identified in affective mode disorders on to the model, and were able to suggest mechanisms by which the mutations caused impairment in channel function [112]. This model was also used in a further study analysing two gain-of-function SNPs in human P2X7 (H155Y and A348T), comparing them with their reciprocal mutations in rat P2X7 [113]. Finally, the same model was

used in a paper comparing the function of the highly homologous human and rhesus macaque P2X7 receptors [114]. In addition, models of hP2X7 based upon PDB IDs 4DW0 and 4DW1 have been used in a review by Jiang *et al* to discuss the molecular mechanisms underlying mammalian P2X7 receptor function, but no details of model construction were provided [115].

4.6 OTHER P2X RECEPTORS

Other P2X receptors that have been modelled from zfP2X4.1 include DdP2XA, both with and without a head domain (neither molecular model agreed with the experimental N-glycosylation analysis data, which is not surprising given the very low sequence identity (16%) between the two receptors) [57], and rP2X5 [12].

4.7 MOLECULAR DYNAMICS SIMULATIONS

Molecular dynamics, where computational methods are used to simulate molecular motions over time, can provide interesting and useful information about protein conformation, and how it changes if the system is perturbed, by placing a molecular model of a membrane protein in a lipid bilayer, or docking a ligand into its binding site. It has been used for P2X receptors both to look at the gating mechanism [10], and to attempt to determine whether or not the ATP-bound crystal structure of zfP2X4.1 is a fair representation of the open-channel state [103, 116]. Du *et al* used both normal mode analysis and molecular dynamics simulations to develop a model for the gating mechanism of zfP2X4.1R [10]. The authors performed normal mode analysis using ElNemo software [117]. Briefly, normal mode analysis involves making elastic connections between each atom and its near neighbours, and allowing the system to oscillate with the same frequency and a fixed phase relation. The object of this experiment was to find conformations of the model which showed the largest widening of the TM pore coupled with the largest closure around the ATP-binding site, to find a model which looked like an open-channel state. Molecular dynamics simulations of the isolated extracellular domain without and with ATP (docked using AutoDock Vina) were carried out using NAMD [118] for 35 ns. Two distinct conformations of ATP in the binding site were observed, but on superficial inspection neither of these conformations resembles the conformation of ATP in the ATP-bound zfP2X4.1 crystal structure [16].

Heymann *et al* performed molecular dynamics simulations of zfP2X4.1 inserted into a model lipid bilayer using VMD software [119] and NAMD, for just less than 80 ns [116]. They showed that over this time period bilayer lipids were able to enter the lateral fenestrations, excluding water from the pore (which would inhibit ion flow through the channel). From this, and their observation that there are relatively few inter-subunit interactions in the TM helices of the ATP-bound zfP2X4.1 crystal structure, they argued that the open-state crystal structure is distorted. They were able to generate a new zfP2X4.1 open-state model in which the TM helices were closer together and the lateral portals were narrowed. This new model

contained more inter-subunit interactions in the TM helices, which the authors argued was a fairer representation of the physiological open-state. In addition, metal bridges were introduced into the receptor (cadmium ions bridging between cysteine residues (either native or introduced)), and the functional data obtained in these experiments was consistent with the TM helix orientations as seen in the *apo*- and ATP-bound crystal structures. Rothwell *et al* used GROMACS software [120], running coarse-grained molecular dynamics simulations to position a model of rat P2X2 within a lipid bilayer, and identifying the environment of Ile-328, situated towards the top of TM2 [103]. They found that lipids intercalated between the TM helices during their simulation, and hypothesised that lipids might be able to stabilise the open state of the receptor. They tested this hypothesis by making a series of cysteine mutants and assessing the effect of labelling with propyl methane thiosulfonate (MTSP), a lipophilic crosslinker, and found that labelling at position 328 was able to open the channel in a manner similar to ATP. From these data they concluded that the ATP-bound zfP2X4.1 crystal structure was a fair reflection of the open-channel state, and that intercalation of lipids between the TM helices played an important role in ion channel function, stabilising the open-channel state.

4.8 MOLECULAR MODELLING: SUMMARY

In summary, the availability of crystal structures as molecular modelling templates has significantly improved both the accuracy and scope of interpretation of structure-function data, and in many cases has allowed for the identification of key regions, clusters and interactions of amino-acid residues which have then been shown by experiment to have significant effects on P2X receptor function. By allowing structure-based experimental design, modelling has also led to interesting developments of altered P2X receptor constructs, which can report on fluorescence changes induced by activation, and can be activated by light or lipophilic attachment. A number of different methods have been used to generate P2X receptor molecular models, but a broad consensus about what works well is emerging; adequate models can be constructed using Modeller software, but some further quality control is necessary, usually using MolProbity and UCSF Chimera for energy minimisation. Because PDB ID 4DW0 corrects a mis-assignment of amino-acid sequence in the original closed-state zfP2X4.1 crystal structures (PDB IDs 3H9V and 3I5D) [16], this is the PDB file which should be used from now on to model the closed-state. Although there have been relatively few studies using molecular dynamics to date, they have uncovered important insights regarding the interaction of lipids with the TM helices, and have proved useful in demonstrating that the ATP-bound crystal structure is a fair approximation of the open-channel state.

5. FUTURE PERSPECTIVES

5.1 WHY MORE HIGH-RESOLUTION STRUCTURES ARE NEEDED

The publication of the high resolution structures of zfP2X4.1 in both the *apo*- and ATP-bound states represents a significant advance in our understanding of the structural biology of P2X receptors. However, we still have no high resolution structures of human or mammalian P2X receptors; these are vital for a full understanding of structure-function relationships and for drug design.

The pharmacological profile and agonist sensitivity of P2X receptors varies considerably among receptor subtypes as well as across species. These differences may be as a result of subtle differences in amino acid sequence which cause slight variations in structure, enabling differential agonist and antagonist binding. For example, α,β-meATP is a potent agonist at P2X1, P2X3 and P2X5 receptors but is inactive at P2X2, P2X4 and P2X7 receptors [121-124]. Additionally α,β-meATP is more potent at rP2X5 (EC_{50} – 1.1 μM) compared with hP2X5 (EC_{50} – 12.2 μM) [124, 125]. Deciphering multiple P2X structures will enable us to compare different subtypes and help us understand the molecular basis of differential agonist binding between subtypes. Moreover, this information will aid the development of new and selective agonists and antagonists at individual receptors using structure-based drug design.

Very little is known regarding the mechanism underlying antagonist binding at P2XRs. In hP2X1, a cluster of positively charged residues at the base of the head domain is proposed to be involved in binding the competitive antagonist, suramin and its derivative NF449 [89]. A structure of a P2X receptor in complex with an antagonist such as PPADS or suramin would aid our understanding of how these molecules block the receptors, as well as why some receptors are sensitive and some resistant to antagonism. This information would assist in the development of new, targeted inhibitors of P2XRs.

There is some evidence that ivermectin, an allosteric modulator of P2X4Rs, potentiates currents through P2X4 receptors by increasing the number of receptors at the cell surface [126]. However, as with glutamate-gated chloride channels [127], ivermectin is also thought to interact with the TM helices of P2X4 to stabilize the open-channel conformation [128, 129]. More recently, ivermectin has also been shown to positively modulate the current at hP2X7, but not at rat or mouse P2X7 [130]. The exact mechanism underlying the binding of ivermectin to these receptors is unknown; therefore solving a P2X structure in complex with ivermectin is of key interest to enhance our level of understanding of how P2XRs are modulated.

The formation of large pores, permeable to molecules of up to 900Da, upon prolonged P2X7 receptor activation is a subject of much speculation. A P2X7 structure in the dilated state would help answer many

of the key questions regarding P2X7 activation, i.e. whether the large pore is formed by P2X7 itself or relies upon activation of an additional channel via second messengers [131].

As previously described, solving the structure of zfP2X4.1 required significant mutagenesis for crystallization. Although the constructs retained some ATP-gated channel function in mammalian cells, the pharmacological profile of the receptor was significantly altered. The mutations introduced into the construct may have some effects on the structure of the channel and therefore it is still necessary to solve the structure of a fully functional channel. Additionally, the N- and C-termini were truncated from the zebrafish structure; therefore we have very little knowledge regarding the structure of these domains which have been shown to be important in desensitization kinetics of P2XRs.

5.2 WHERE ARE NEW STRUCTURES LIKELY TO COME FROM?

Commonly used systems for membrane protein expression include expression in bacterial systems such as *E. coli* as well as eukaryotic expression systems including yeast, insect cells and mammalian cells.

Expression of full length P2X receptors in *E. coli* has proved to be largely unsuccessful with the majority of the protein becoming mis-folded and being degraded. An alternative to the expression of a full-length protein is heterologous expression of an individual receptor domain (e.g. the extracellular domain) to improve protein solubilisation. Following expression of the extracellular domain in *E. coli*, it can be extracted from inclusion bodies and refolded. This method has been used successfully for the expression and refolding of the extracellular domains of rP2X2, rP2X4 and hP2X7 [132-134], but as yet, no structures of these domains have been published. Structures of P2X receptor extracellular domains would be particularly suited to the identification of agonist and antagonist binding sites, aiding structure based drug design (assuming that they formed trimers).

The C-terminal domain of rP2X2 has also been expressed in *E. coli*. The isolated C-terminus was extracted from *E. coli* and mixed with a rat brain protein lysate to perform a pull-down assay. The aim of this work was to identify P2X2 C-terminal domain interacting proteins using mass spectrometry [135]. Expressing and solving the structure of the isolated C-terminus would give insight into other protein interactions and docking analysis.

The use of yeast for the expression of full length P2X receptors has also been largely unsuccessful [136]. All the structural work published to date, including the crystal structures of zfP2X4.1, has been based on protein expressed and purified from baculovirus-infected insect cells or mammalian cells, indicating that these expression systems are likely to be most successful in the future for P2XR expression and purification.

The use of HEK293S GNTI(-) cells is becoming increasingly widespread for membrane protein expression. This specialized cell line lacks the N-acetylglucosaminyltransferase (GnTI) enzyme, thereby diminishing the formation of complex N-glycans [137]. Therefore the use of these cells provides a platform for the production of a homogeneous population of membrane protein. The structure of TRPV1 has recently been solved to a resolution of 3.4 Å, following expression in HEK-293 GNTI(-) cells, without protein crystallisation through the use of single particle cryo-EM and a direct electron detector [81]. This breakthrough in structural biology demonstrates that it might be possible to solve P2XR structures (particularly for the large subtypes P2X2 and P2X7) using these techniques without the need for crystallisation.

6. CONCLUDING REMARKS

This review demonstrates the vital contribution of the crystal structures of zfP2X4.1 in the *apo*- and ATP-bound states to our understanding of the P2X receptor structure-function relationship. It is also clear that the crystal structures have been validated, not only by a large body of previous data, but also by recent experiments designed based upon molecular models derived from them. In our opinion, the largest uncertainties in the crystal structure lie in the precise positioning of the TM helices, particularly in the ATP-bound state, but this is perhaps not surprising given that (i) in order to obtain well-diffracting crystals suitable for structural study, the intracellular N- and C-terminal domains (known to be important for receptor function) had to be truncated, and (ii) the quality of electron density in this region of the crystal structure was relatively poor compared to that in the extracellular domain.

A question remains regarding how representative zfP2X4.1 is of the more widely-studied mammalian P2X receptors. A detailed study of zfP2X4.1 channel properties and pharmacology would be very useful in this regard to aid comparison, but it is clear that the overall 3D-structures of zfP2X4.1 and the mammalian P2X receptors are very similar. However, it is important to note that, with amino-acid identity between the regions of zfP2X4.1 encompassed by the crystal structures and the human P2X receptors ranging from 45% to 62%, molecular models should be interpreted with some caution. With this in mind, however, the molecular models that have been made so far have been incredibly useful in interpretation of data, and the few molecular dynamics simulations performed to date have highlighted some very interesting phenomena, particularly the intercalation of membrane lipids into the TM helices. In our opinion this is clearly an area which merits further exploration.

Finally, despite the huge advances made in solving the *apo*- and ATP-bound crystal structures of zfP2X4.1, we still do not understand the structural basis for differential agonist potency, allosteric modulation, pore dilatation or desensitization, and consequently more structures are needed. However,

given the difficulty associated with expression of mammalian P2X receptors for structural studies, the acquisition of new structures remains a significant challenge to the research field.

ABBREVIATIONS

GFP, Green fluorescent protein; ATP , adenosine-5'-triphosphate; BzATP , 2'(3')-O-(4-Benzoylbenzoyl) adenosine-5'-triphosphate; αβmeATP , α,β-Methyleneadenosine 5′-triphosphate; PPADS , pyridoxalphosphate-6-azophenyl-2',4'-disulfonic acid; FSEC , fluorescence size exclusion chromatography; PKC , protein kinase C; TM , transmembrane; ASIC , acid sensing ion channel; NTD , amino terminal domain; AFM , atomic force microscopy; TEM, transmission electron microscopy; TMRM, tetramethyl rhodamine maleimide; MTSET, 2-(trimethylammonium)ethyl methane thiosulfonate; MTSP, propyl methane thiosulfonate; GNTI, N-acetylglucosaminyltransferase.

ACKNOWLEDGEMENTS

MTY was supported by an Evans-Huber Fellowship from Cardiff University. LG was supported by a BBSRC/MRC PhD studentship.

REFERENCES

[1] Brake, A.J.; Wagenbach, M.J.; Julius, D. New structural motif for ligand-gated ion channels defined by an ionotropic ATP receptor. *Nature,* **1994**, *371*(6497), 519-523.

[2] Valera, S.; Hussy, N.; Evans, R.J.; Adami, N.; North, R.A.; Surprenant, A.; Buell, G. A new class of ligand-gated ion channel defined by P2x receptor for extracellular ATP. *Nature,* **1994**, *371*(6497), 516-519.

[3] Surprenant, A.; North, R.A. Signaling at Purinergic P2X Receptors. *Annu. Rev. Physiol.,* **2009**, *71*(1), 333-359.

[4] Kawate, T.; Michel, J.C.; Birdsong, W.T.; Gouaux, E. Crystal structure of the ATP-gated P2X4 ion channel in the closed state. *Nature,* **2009**, *460*(7255), 592-598.

[5] Silberberg, S.D.; Swartz, K.J. Structural biology: Trimeric ion-channel design. *Nature,* **2009**, *460*(7255), 580-581.

[6] Browne, L.E.; Jiang, L.H.; North, R.A. New structure enlivens interest in P2X receptors. *Trends Pharmacol. Sci.,* **2010**, *31*(5), 229-237.

[7] Evans, R.J. Structural interpretation of P2X receptor mutagenesis studies on drug action. *Br. J. Pharmacol.,* **2010**, *161*(5), 961-971.

[8] Young, M.T. P2X receptors: dawn of the post-structure era. *Trends Biochem. Sci.,* **2010**, *35*(2), 83-90.

[9] Browne, L.E.; Cao, L.; Broomhead, H.E.; Bragg, L.; Wilkinson, W.J.; North, R.A. P2X receptor channels show threefold symmetry in ionic charge selectivity and unitary conductance. *Nat. Neurosci.,* **2011**, *14*(1), 17-18.

[10] Du, J.; Dong, H.; Zhou, H.X. Gating mechanism of a P2X4 receptor developed from normal mode analysis and molecular dynamics simulations. *Proc. Natl. Acad. Sci. USA,* **2012**, *109*(11), 4140-4145.

[11] Jiang, R.; Lemoine, D.; Martz, A.; Taly, A.; Gonin, S.; Prado de Carvalho, L.; Specht, A.; Grutter, T. Agonist trapped in ATP-binding sites of the P2X2 receptor. *Proc. Natl. Acad. Sci. USA,* **2011**, *108*(22), 9066-9071.

[12] Kawate, T.; Robertson, J.L.; Li, M.; Silberberg, S.D.; Swartz, K.J. Ion access pathway to the transmembrane pore in P2X receptor channels. *J. Gen. Physiol.,* **2011**, *137*(6), 579-590.

[13] Li, M.; Kawate, T.; Silberberg, S.D.; Swartz, K.J. Pore-opening mechanism in trimeric P2X receptor channels. *Nat. Commun.,* **2010**, *1*, 44.

[14] Roberts, J.A.; Allsopp, R.C.; El Ajouz, S.; Vial, C.; Schmid, R.; Young, M.T.; Evans, R.J. Agonist binding evokes extensive conformational changes in the extracellular domain of the ATP-gated human P2X1 receptor ion channel. *Proc. Natl. Acad. Sci. USA,* **2012**, *109*(12), 4663-4667.

[15] Samways, D.S.; Khakh, B.S.; Dutertre, S.; Egan, T.M. Preferential use of unobstructed lateral portals as the access route to the pore of human ATP-gated ion channels (P2X receptors). *Proc. Natl. Acad. Sci. USA,* **2011**, *108*(33), 13800-13805.

[16] Hattori, M.; Gouaux, E. Molecular mechanism of ATP binding and ion channel activation in P2X receptors. *Nature,* **2012**, *485*(7397), 207-212.

[17] Alves, L.A.; da Silva, J.H.; Ferreira, D.N.; Fidalgo-Neto, A.A.; Teixeira, P.C.; de Souza, C.A.; Caffarena, E.R.; de Freitas, M.S. Structural and Molecular Modeling Features of P2X Receptors. *Int. J. Mol. Sci.,* **2014**, *15*(3), 4531-4549.

[18] Jiang, R.; Taly, A.; Grutter, T. Moving through the gate in ATP-activated P2X receptors. *Trends Biochem. Sci.,* **2013**, *38*(1), 20-29.

[19] North, R.A.; Jarvis, M.F. P2X receptors as drug targets. *Mol. Pharmacol.,* **2013**, *83*(4), 759-769.

[20] Samways, D.S.; Li, Z.; Egan, T.M. Principles and properties of ion flow in P2X receptors. *Front. Cell. Neurosci.,* **2014**, *8*, 6.

[21] Kucenas, S.; Li, Z.; Cox, J.A.; Egan, T.M.; Voigt, M.M. Molecular characterization of the zebrafish P2X receptor subunit gene family. *Neuroscience,* **2003**, *121*(4), 935-945.

[22] Diaz-Hernandez, M.; Cox, J.A.; Migita, K.; Haines, W.; Egan, T.M.; Voigt, M.M. Cloning and characterization of two novel zebrafish P2X receptor subunits. *Biochem. Biophys. Res. Commun.,* **2002**, *295*(4), 849-853.
[23] North, R.A. Molecular physiology of P2X receptors. *Physiol. Rev.,* **2002**, *82*(4), 1013-1067.
[24] Buell, G.; Lewis, C.; Collo, G.; North, R.A.; Surprenant, A. An antagonist-insensitive P2X receptor expressed in epithelia and brain. *EMBO. J.,* **1996**, *15*(1), 55-62.
[25] Khakh, B.S.; Burnstock, G.; Kennedy, C.; King, B.F.; North, R.A.; Seguela, P.; Voigt, M.; Humphrey, P.P. International union of pharmacology. XXIV. Current status of the nomenclature and properties of P2X receptors and their subunits. *Pharmacol. Rev.,* **2001**, *53*(1), 107-118.
[26] Jones, C.A.; Chessell, I.P.; Simon, J.; Barnard, E.A.; Miller, K.J.; Michel, A.D.; Humphrey, P.P. Functional characterization of the P2X(4) receptor orthologues. *Br. J. Pharmacol.,* **2000**, *129*(2), 388-394.
[27] Walker, J.E.; Saraste, M.; Runswick, M.J.; Gay, N.J. Distantly related sequences in the alpha- and beta-subunits of ATP synthase, myosin, kinases and other ATP-requiring enzymes and a common nucleotide binding fold. *EMBO J.,* **1982**, *1*(8), 945-951.
[28] Ennion, S.; Hagan, S.; Evans, R.J. The role of positively charged amino acids in ATP recognition by human P2X1 receptors. *J. Biol. Chem.,* **2000**, *275*(45), 35656.
[29] Jiang, L.H.; Rassendren, F.; Surprenant, A.; North, R.A. Identification of amino acid residues contributing to the ATP-binding site of a purinergic P2X receptor. *J. Biol. Chem.,* **2000**, *275*(44), 34190-34196.
[30] Allsopp, R.C.; El Ajouz, S.; Schmid, R.; Evans, R.J. Cysteine scanning mutagenesis (residues Glu52-Gly96) of the human P2X1 receptor for ATP: mapping agonist binding and channel gating. *J. Biol. Chem.,* **2011**, *286*(33), 29207-29217.
[31] Bodnar, M.; Wang, H.; Riedel, T.; Hintze, S.; Kato, E.; Fallah, G.; Groger-Arndt, H.; Giniatullin, R.; Grohmann, M.; Hausmann, R.; Schmalzing, G.; Illes, P.; Rubini, P. Amino acid residues constituting the agonist binding site of the human P2X3 receptor. *J. Biol. Chem.,* **2011**, *286*(4), 2739-2749.
[32] Roberts, J.A.; Digby, H.R.; Kara, M.; Ajouz, S.E.; Sutcliffe, M.J.; Evans, R.J. Cysteine Substitution Mutagenesis and the Effects of Methanethiosulfonate Reagents at P2X2 and P2X4 Receptors Support a Core Common Mode of ATP Action at P2X Receptors. *J. Biol. Chem.,* **2008**, *283*(29), 20126-20136.
[33] Wilkinson, W.J.; Jiang, L.H.; Surprenant, A.; North, R.A. Role of ectodomain lysines in the subunits of the heteromeric P2X2/3 receptor. *Mol. Pharmacol.,* **2006**, *70*(4), 1159-1163.
[34] Roberts, J.A.; Evans, R.J. Cysteine substitution mutants give structural insight and identify ATP binding and activation sites at P2X receptors. *J. Neurosci.,* **2007**, *27*(15), 4072-4082.
[35] Worthington, R.A.; Smart, M.L.; Gu, B.J.; Williams, D.A.; Petrou, S.; Wiley, J.S.; Barden, J.A. Point mutations confer loss of ATP-induced human P2X(7) receptor function. *FEBS Lett.,* **2002**, *512*(1-3), 43-46.
[36] Fischer, W.; Zadori, Z.; Kullnick, Y.; Groger-Arndt, H.; Franke, H.; Wirkner, K.; Illes, P.; Mager, P.P. Conserved lysin and arginin residues in the extracellular loop of P2X(3) receptors are involved in agonist binding. *Eur. J. Pharmacol.,* **2007**, *576*(1-3), 7-17.
[37] Zemkova, H.; Yan, Z.; Liang, Z.; Jelinkova, I.; Tomic, M.; Stojilkovic, S.S. Role of aromatic and charged ectodomain residues in the P2X(4) receptor functions. *J. Neurochem.,* **2007**, *102*(4), 1139-1150.
[38] Marquez-Klaka, B.; Rettinger, J.; Bhargava, Y.; Eisele, T.; Nicke, A. Identification of an intersubunit cross-link between substituted cysteine residues located in the putative ATP binding site of the P2X1 receptor. *J. Neurosci.,* **2007**, *27*(6), 1456-1466.
[39] Marquez-Klaka, B.; Rettinger, J.; Nicke, A. Inter-subunit disulfide cross-linking in homomeric and heteromeric P2X receptors. *Eur. Biophys. J.,* **2009**, *38*(3), 329-338.
[40] Chataigneau, T.; Lemoine, D.; Grutter, T. Exploring the ATP-binding site of P2X receptors. *Front. Cell. Neurosci.,* **2013**, *7*, 273.
[41] Coddou, C.; Yan, Z.; Obsil, T.; Huidobro-Toro, J.P.; Stojilkovic, S.S. Activation and regulation of purinergic P2X receptor channels. *Pharmacol. Rev.,* **2011**, *63*(3), 641-683.

[42] Wildman, S.S.; Brown, S.G.; King, B.F.; Burnstock, G. Selectivity of diadenosine polyphosphates for rat P2X receptor subunits. *Eur. J. Pharmacol.,* **1999**, *367*(1), 119-123.
[43] Egan, T.M.; Khakh, B.S. Contribution of calcium ions to P2X channel responses. *J. Neurosci.,* **2004**, *24*(13), 3413-3420.
[44] Virginio, C.; North, R.A.; Surprenant, A. Calcium permeability and block at homomeric and heteromeric P2X2 and P2X3 receptors, and P2X receptors in rat nodose neurones. *J. Physiol.,* **1998**, *510(Pt 1)*, 27-35.
[45] Ding, S.; Sachs, F. Ion permeation and block of P2X(2) purinoceptors: single channel recordings. *J. Membr. Biol.,* **1999**, *172*(3), 215-223.
[46] Migita, K.; Haines, W.R.; Voigt, M.M.; Egan, T.M. Polar residues of the second transmembrane domain influence cation permeability of the ATP-gated P2X(2) receptor. *J. Biol. Chem.,* **2001**, *276*(33), 30934-30941.
[47] Egan, T.M.; Haines, W.R.; Voigt, M.M. A domain contributing to the ion channel of ATP-gated P2X2 receptors identified by the substituted cysteine accessibility method. *J. Neurosci.,* **1998**, *18*(7), 2350-2359.
[48] Rassendren, F.; Buell, G.; Newbolt, A.; North, R.A.; Surprenant, A. Identification of amino acid residues contributing to the pore of a P2X receptor. *EMBO J.,* **1997**, *16*(12), 3446-3454.
[49] Cao, L.; Young, M.T.; Broomhead, H.E.; Fountain, S.J.; North, R.A. Thr339-to-serine substitution in rat P2X2 receptor second transmembrane domain causes constitutive opening and indicates a gating role for Lys308. *J. Neurosci.,* **2007**, *27*(47), 12916-12923.
[50] Boue-Grabot, E.; Archambault, V.; Seguela, P. A protein kinase C site highly conserved in P2X subunits controls the desensitization kinetics of P2X(2) ATP-gated channels. *J. Biol. Chem.,* **2000**, *275*(14), 10190-10195.
[51] Wen, H.; Evans, R.J. Regions of the amino terminus of the P2X receptor required for modification by phorbol ester and mGluR1alpha receptors. *J. Neurochem.,* **2009**, *108*(2), 331-340.
[52] Allsopp, R.C.; Farmer, L.K.; Fryatt, A.G.; Evans, R.J. P2X receptor chimeras highlight roles of the amino terminus to partial agonist efficacy, the carboxyl terminus to recovery from desensitization, and independent regulation of channel transitions. *J. Biol. Chem.,* **2013**, *288*(29), 21412-21421.
[53] Allsopp, R.C.; Evans, R.J. The intracellular amino terminus plays a dominant role in desensitization of ATP-gated P2X receptor ion channels. *J. Biol. Chem.,* **2011**, *286*(52), 44691-44701.
[54] Chaumont, S.; Jiang, L.H.; Penna, A.; North, R.A.; Rassendren, F. Identification of a trafficking motif involved in the stabilization and polarization of P2X receptors. *J. Biol. Chem.,* **2004**, *279*(28), 29628-29638.
[55] Royle, S.J.; Bobanovic, L.K.; Murrell-Lagnado, R.D. Identification of a non-canonical tyrosine-based endocytic motif in an ionotropic receptor. *J. Biol. Chem.,* **2002**, *277*(38), 35378-35385.
[56] Ennion, S.J.; Evans, R.J. Conserved cysteine residues in the extracellular loop of the human P2X(1) receptor form disulfide bonds and are involved in receptor trafficking to the cell surface. *Mol. Pharmacol.,* **2002**, *61*(2), 303-311.
[57] Valente, M.; Watterson, S.J.; Parker, M.D.; Ford, R.C.; Young, M.T. Expression, purification, electron microscopy, N-glycosylation mutagenesis and molecular modeling of human P2X4 and Dictyostelium discoideum P2XA. *Biochim. Biophys. Acta,* **2011**, *1808*(12), 2859-2866.
[58] Wang, H.; Elferich, J.; Gouaux, E. Structures of LeuT in bicelles define conformation and substrate binding in a membrane-like context. *Nat. Struct. Mol. Biol.,* **2012**, *19*(2), 212-219.
[59] Kracun, S.; Chaptal, V.; Abramson, J.; Khakh, B.S. Gated access to the pore of a P2X receptor: structural implications for closed-open transitions. *J. Biol. Chem.,* **2010**, *285*(13), 10110-10121.
[60] Samways, D.S.; Khakh, B.S.; Egan, T.M. Allosteric modulation of Ca2+ flux in ligand-gated cation channel (P2X4) by actions on lateral portals. *J. Biol. Chem.,* **2012**, *287*(10), 7594-7602.
[61] Gonzales, E.B.; Kawate, T.; Gouaux, E. Pore architecture and ion sites in acid-sensing ion channels and P2X receptors. *Nature,* **2009**, *460*(7255), 599-604.
[62] Jasti, J.; Furukawa, H.; Gonzales, E.B.; Gouaux, E. Structure of acid-sensing ion channel 1 at 1.9 A resolution and low pH. *Nature,* **2007**, *449*(7160), 316-323.

[63] Paukert, M.; Babini, E.; Pusch, M.; Grunder, S. Identification of the Ca2+ blocking site of acid-sensing ion channel (ASIC) 1: implications for channel gating. *J. Gen. Physiol.,* **2004**, *124*(4), 383-394.
[64] Silberberg, S.D.; Chang, T.H.; Swartz, K.J. Secondary structure and gating rearrangements of transmembrane segments in rat P2X4 receptor channels. *J. Gen. Physiol.,* **2005**, *125*(4), 347-359.
[65] Champigny, G.; Voilley, N.; Waldmann, R.; Lazdunski, M. Mutations causing neurodegeneration in Caenorhabditis elegans drastically alter the pH sensitivity and inactivation of the mammalian H+-gated Na+ channel MDEG1. *J. Biol. Chem.,* **1998**, *273*(25), 15418-15422.
[66] Cushman, K.A.; Marsh-Haffner, J.; Adelman, J.P.; McCleskey, E.W. A conformation change in the extracellular domain that accompanies desensitization of acid-sensing ion channel (ASIC) 3. *J. Gen. Physiol.,* **2007**, *129*(4), 345-350.
[67] Dawson, R.J.; Benz, J.; Stohler, P.; Tetaz, T.; Joseph, C.; Huber, S.; Schmid, G.; Hugin, D.; Pflimlin, P.; Trube, G.; Rudolph, M.G.; Hennig, M.; Ruf, A. Structure of the acid-sensing ion channel 1 in complex with the gating modifier Psalmotoxin 1. *Nat. Commun.,* **2012**, *3*, 936.
[68] Baconguis, I.; Hattori, M.; Gouaux, E. Unanticipated parallels in architecture and mechanism between ATP-gated P2X receptors and acid sensing ion channels. *Curr. Opin. Struct. Biol.,* **2013**, *23*(2), 277-284.
[69] Baconguis, I.; Gouaux, E. Structural plasticity and dynamic selectivity of acid-sensing ion channel-spider toxin complexes. *Nature,* **2012**, *489*(7416), 400-405.
[70] Barrera, N.P.; Henderson, R.M.; Edwardson, J.M. Determination of the architecture of ionotropic receptors using AFM imaging. *Pflugers. Arch.,* **2008**, *456*(1), 199-209.
[71] Barrera, N.P.; Henderson, R.M.; Murrell-Lagnado, R.D.; Edwardson, J.M. The stoichiometry of P2X2/6 receptor heteromers depends on relative subunit expression levels. *Biophys. J.,* **2007**, *93*(2), 505-512.
[72] Barrera, N.P.; Ormond, S.J.; Henderson, R.M.; Murrell-Lagnado, R.D.; Edwardson, J.M. Atomic force microscopy imaging demonstrates that P2X2 receptors are trimers but that P2X6 receptor subunits do not oligomerize. *J. Biol. Chem.,* **2005**, *280*(11), 10759-10765.
[73] Nakazawa, K.; Yamakoshi, Y.; Tsuchiya, T.; Ohno, Y. Purification and aqueous phase atomic force microscopic observation of recombinant P2X2 receptor. *Eur. J. Pharmacol.,* **2005**, *518*(2-3), 107-110.
[74] Shinozaki, Y.; Sumitomo, K.; Tsuda, M.; Koizumi, S.; Inoue, K.; Torimitsu, K. Direct Observation of ATP-Induced Conformational Changes in Single P2X4 Receptors. *PLoS. Biol.,* **2009**, *7*(5), e103.
[75] Mio, K.; Kubo, Y.; Ogura, T.; Yamamoto, T.; Sato, C. Visualization of the trimeric P2X2 receptor with a crown-capped extracellular domain. *Biochem. Biophys. Res. Commun.,* **2005**, *337*(3), 998-1005.
[76] Mio, K.; Ogura, T.; Yamamoto, T.; Hiroaki, Y.; Fujiyoshi, Y.; Kubo, Y.; Sato, C. Reconstruction of the P2X(2) receptor reveals a vase-shaped structure with lateral tunnels above the membrane. *Structure,* **2009**, *17*(2), 266-275.
[77] Young, M.T.; Fisher, J.A.; Fountain, S.J.; Ford, R.C.; North, R.A.; Khakh, B.S. Molecular Shape, Architecture, and Size of P2X4 Receptors Determined Using Fluorescence Resonance Energy Transfer and Electron Microscopy. *J. Biol. Chem.,* **2008**, *283*(38), 26241-26251.
[78] Kawate, T.; Gouaux, E. Fluorescence-detection size-exclusion chromatography for precrystallization screening of integral membrane proteins. *Structure,* **2006**, *14*(4), 673-681.
[79] Frank, J. *Three-dimensional electron microscopy of macromolecular assemblies*. Second edition ed. Oxford University Press, **2006**.
[80] Cao, E.; Liao, M.; Cheng, Y.; Julius, D. TRPV1 structures in distinct conformations reveal activation mechanisms. *Nature,* **2013**, *504*(7478), 113-118.
[81] Liao, M.; Cao, E.; Julius, D.; Cheng, Y. Structure of the TRPV1 ion channel determined by electron cryo-microscopy. *Nature,* **2013**, *504*(7478), 107-112.
[82] Mosimann, S.; Meleshko, R.; James, M.N. A critical assessment of comparative molecular modeling of tertiary structures of proteins. *Proteins,* **1995**, *23*(3), 301-317.

[83] Forrest, L.R.; Tang, C.L.; Honig, B. On the accuracy of homology modeling and sequence alignment methods applied to membrane proteins. *Biophys. J.,* **2006**, *91*(2), 508-517.
[84] Lomize, M.A.; Lomize, A.L.; Pogozheva, I.D.; Mosberg, H.I. OPM: orientations of proteins in membranes database. *Bioinformatics,* **2006**, *22*(5), 623-625.
[85] Webb, B.; Sali, A. Protein Structure Modeling with MODELLER. *Methods Mol. Biol.,* **2014**, *1137*, 1-15.
[86] Hooft, R.W.; Vriend, G.; Sander, C.; Abola, E.E. Errors in protein structures. *Nature,* **1996**, *381*(6580), 272.
[87] Wiederstein, M.; Sippl, M.J. ProSA-web: interactive web service for the recognition of errors in three-dimensional structures of proteins. *Nucleic Acids Res.,* **2007**, *35*, 407-410.
[88] Verdonk, M.L.; Cole, J.C.; Hartshorn, M.J.; Murray, C.W.; Taylor, R.D. Improved protein-ligand docking using GOLD. *Proteins,* **2003**, *52*(4), 609-623.
[89] El-Ajouz, S.; Ray, D.; Allsopp, R.C.; Evans, R.J. Molecular basis of selective antagonism of the P2X1 receptor for ATP by NF449 and suramin: contribution of basic amino acids in the cysteine-rich loop. *Br. J. Pharmacol.,* **2012**, *165*(2), 390-400.
[90] Lorinczi, E.; Bhargava, Y.; Marino, S.F.; Taly, A.; Kaczmarek-Hajek, K.; Barrantes-Freer, A.; Dutertre, S.; Grutter, T.; Rettinger, J.; Nicke, A. Involvement of the cysteine-rich head domain in activation and desensitization of the P2X1 receptor. *Proc. Natl. Acad. Sci. USA,* **2012**, *109*(28), 11396-11401.
[91] Cao, L.; Broomhead, H.E.; Young, M.T.; North, R.A. Polar residues in the second transmembrane domain of the rat P2X2 receptor that affect spontaneous gating, unitary conductance, and rectification. *J. Neurosci.,* **2009**, *29*(45), 14257-14264.
[92] Keceli, B.; Kubo, Y. Functional and structural identification of amino acid residues of the P2X2 receptor channel critical for the voltage- and [ATP]-dependent gating. *J. Physiol.,* **2009**, *587*(Pt 24), 5801-5818.
[93] Arnold, K.; Bordoli, L.; Kopp, J.; Schwede, T. The SWISS-MODEL workspace: a web-based environment for protein structure homology modelling. *Bioinformatics,* **2006**, *22*(2), 195-201.
[94] Bordoli, L.; Kiefer, F.; Arnold, K.; Benkert, P.; Battey, J.; Schwede, T. Protein structure homology modeling using SWISS-MODEL workspace. *Nat. Protoc.,* **2009**, *4*(1), 1-13.
[95] Jiang, R.; Martz, A.; Gonin, S.; Taly, A.; de Carvalho, L.P.; Grutter, T. A putative extracellular salt bridge at the subunit interface contributes to the ion channel function of the ATP-gated P2X2 receptor. *J. Biol. Chem.,* **2010**, *285*(21), 15805-15815.
[96] Emsley, P.; Cowtan, K. Coot: model-building tools for molecular graphics. *Acta Crystallogr. D. Biol. Crystallogr.,* **2004**, *60*(Pt 12 Pt 1), 2126-2132.
[97] Murshudov, G.N.; Vagin, A.A.; Dodson, E.J. Refinement of macromolecular structures by the maximum-likelihood method. *Acta Crystallogr. D. Biol. Crystallogr.,* **1997**, *53*(Pt 3), 240-255.
[98] Chen, V.B.; Arendall, W.B., 3rd; Headd, J.J.; Keedy, D.A.; Immormino, R.M.; Kapral, G.J.; Murray, L.W.; Richardson, J.S.; Richardson, D.C. MolProbity: all-atom structure validation for macromolecular crystallography. *Acta Crystallogr. D. Biol. Crystallogr.,* **2010**, *66*(Pt 1), 12-21.
[99] Pettersen, E.F.; Goddard, T.D.; Huang, C.C.; Couch, G.S.; Greenblatt, D.M.; Meng, E.C.; Ferrin, T.E. UCSF Chimera--a visualization system for exploratory research and analysis. *J. Comput. Chem.,* **2004**, *25*(13), 1605-1612.
[100] Wolf, C.; Rosefort, C.; Fallah, G.; Kassack, M.U.; Hamacher, A.; Bodnar, M.; Wang, H.; Illes, P.; Kless, A.; Bahrenberg, G.; Schmalzing, G.; Hausmann, R. Molecular determinants of potent P2X2 antagonism identified by functional analysis, mutagenesis, and homology docking. *Mol. Pharmacol.,* **2011**, *79*(4), 649-661.
[101] Punthambaker, S.; Blum, J.A.; Hume, R.I. High potency zinc modulation of human P2X2 receptors and low potency zinc modulation of rat P2X2 receptors share a common molecular mechanism. *J. Biol. Chem.,* **2012**, *287*(26), 22099-22111.
[102] Stelmashenko, O.; Compan, V.; Browne, L.E.; North, R.A. Ectodomain Movements of an ATP-gated Ion Channel (P2X2 receptor) Probed by Disulfide Locking. *J. Biol. Chem.,* **2014**.

[103] Rothwell, S.W.; Stansfeld, P.J.; Bragg, L.; Verkhratsky, A.; North, R.A. Direct Gating of ATP-activated Ion Channels (P2X2 Receptors) by Lipophilic Attachment at the Outer End of the Second Transmembrane Domain. *J. Biol. Chem.,* **2014**, *289*(2), 618-626.
[104] Browne, L.E.; Nunes, J.P.; Sim, J.A.; Chudasama, V.; Bragg, L.; Caddick, S.; Alan North, R. Optical control of trimeric P2X receptors and acid-sensing ion channels. *Proc. Natl. Acad. Sci. USA,* **2014**, *111*(1), 521-526.
[105] Lemoine, D.; Habermacher, C.; Martz, A.; Mery, P.F.; Bouquier, N.; Diverchy, F.; Taly, A.; Rassendren, F.; Specht, A.; Grutter, T. Optical control of an ion channel gate. *Proc. Natl. Acad. Sci. USA,* **2013**, *110*(51), 20813-20818.
[106] Laskowski, R.A.; Macarthur, M.W.; Moss, D.S.; Thornton, J.M. Procheck - a Program to Check the Stereochemical Quality of Protein Structures. *J. Appl. Crystallogr.,* **1993**, *26*, 283-291.
[107] Jindrichova, M.; Khafizov, K.; Skorinkin, A.; Fayuk, D.; Bart, G.; Zemkova, H.; Giniatullin, R. Highly conserved tyrosine 37 stabilizes desensitized states and restricts calcium permeability of ATP-gated P2X3 receptor. *J. Neurochem.,* **2011**, *119*(4), 676-685.
[108] Petrenko, N.; Khafizov, K.; Tvrdonova, V.; Skorinkin, A.; Giniatullin, R. Role of the ectodomain serine 275 in shaping the binding pocket of the ATP-gated P2X3 receptor. *Biochemistry,* **2011**, *50*(39), 8427-8436.
[109] Riedel, T.; Wiese, S.; Leichsenring, A.; Illes, P. Effects of nucleotide analogs at the P2X3 receptor and its mutants identify the agonist binding pouch. *Mol. Pharmacol.,* **2012**, *82*(1), 80-89.
[110] Li, M.; Silberberg, S.D.; Swartz, K.J. Subtype-specific control of P2X receptor channel signaling by ATP and Mg2+. *Proc. Natl. Acad. Sci. USA,* **2013**, *110*(36), E3455-3463.
[111] Fiser, A.; Sali, A. ModLoop: automated modeling of loops in protein structures. *Bioinformatics,* **2003**, *19*(18), 2500-2501.
[112] Roger, S.; Mei, Z.Z.; Baldwin, J.M.; Dong, L.; Bradley, H.; Baldwin, S.A.; Surprenant, A.; Jiang, L.H. Single nucleotide polymorphisms that were identified in affective mood disorders affect ATP-activated P2X7 receptor functions. *J. Psychiatr. Res.,* **2010**, *44*(6), 347-355.
[113] Bradley, H.J.; Baldwin, J.M.; Goli, G.R.; Johnson, B.; Zou, J.; Sivaprasadarao, A.; Baldwin, S.A.; Jiang, L.H. Residues 155 and 348 contribute to the determination of P2X7 receptor function via distinct mechanisms revealed by single-nucleotide polymorphisms. *J. Biol. Chem.,* **2011**, *286*(10), 8176-8187.
[114] Bradley, H.J.; Browne, L.E.; Yang, W.; Jiang, L.H. Pharmacological properties of the rhesus macaque monkey P2X7 receptor. *Br. J. Pharmacol.,* **2011**, *164*(2b), 743-754.
[115] Jiang, L.H.; Baldwin, J.M.; Roger, S.; Baldwin, S.A. Insights into the Molecular Mechanisms Underlying Mammalian P2X7 Receptor Functions and Contributions in Diseases, Revealed by Structural Modeling and Single Nucleotide Polymorphisms. *Front. Pharmacol.,* **2013**, *4*, 55.
[116] Heymann, G.; Dai, J.; Li, M.; Silberberg, S.D.; Zhou, H.X.; Swartz, K.J. Inter- and intrasubunit interactions between transmembrane helices in the open state of P2X receptor channels. *Proc. Natl. Acad. Sci. USA,* **2013**, *110*(42), E4045-4054.
[117] Suhre, K.; Sanejouand, Y.H. ElNemo: a normal mode web server for protein movement analysis and the generation of templates for molecular replacement. *Nucleic Acids Res.,* **2004**, *32*, W610-614.
[118] Phillips, J.C.; Braun, R.; Wang, W.; Gumbart, J.; Tajkhorshid, E.; Villa, E.; Chipot, C.; Skeel, R.D.; Kale, L.; Schulten, K. Scalable molecular dynamics with NAMD. *J. Comput. Chem.,* **2005**, *26*(16), 1781-1802.
[119] Humphrey, W.; Dalke, A.; Schulten, K. VMD: visual molecular dynamics. *J. Mol. Graph.,* **1996**, *14*(1), 33-38, 27-38.
[120] Stansfeld, P.J.; Jefferys, E.E.; Sansom, M.S. Multiscale simulations reveal conserved patterns of lipid interactions with aquaporins. *Structure,* **2013**, *21*(5), 810-819.
[121] Evans, R.J.; Lewis, C.; Buell, G.; Valera, S.; North, R.A.; Surprenant, A. Pharmacological characterization of heterologously expressed ATP-gated cation channels (P2x purinoceptors). *Mol. Pharmacol.,* **1995**, *48*(2), 178-183.
[122] Garcia-Guzman, M.; Stuhmer, W.; Soto, F. Molecular characterization and pharmacological properties of the human P2X3 purinoceptor. *Mol. Brain Res.,* **1997**, *47*(1-2), 59-66.

[123] Norenberg, W.; Illes, P. Neuronal P2X receptors: localisation and functional properties. *Naunyn-Schmiedeberg's Arch. Pharmacol.,* **2000**, *362*(4-5), 324-339.
[124] Wildman, S.S.; Brown, S.G.; Rahman, M.; Noel, C.A.; Churchill, L.; Burnstock, G.; Unwin, R.J.; King, B.F. Sensitization by extracellular Ca(2+) of rat P2X(5) receptor and its pharmacological properties compared with rat P2X(1). *Mol. Pharmacol.,* **2002**, *62*(4), 957-966.
[125] Bo, X.; Jiang, L.H.; Wilson, H.L.; Kim, M.; Burnstock, G.; Surprenant, A.; North, R.A. Pharmacological and biophysical properties of the human P2X5 receptor. *Mol. Pharmacol.,* **2003**, *63*(6), 1407-1416.
[126] Toulme, E.; Soto, F.; Garret, M.; Boue-Grabot, E. Functional properties of internalization-deficient P2X4 receptors reveal a novel mechanism of ligand-gated channel facilitation by ivermectin. *Mol. Pharmacol.,* **2006**, *69*(2), 576-587.
[127] Hibbs, R.E.; Gouaux, E. Principles of activation and permeation in an anion-selective Cys-loop receptor. *Nature,* **2011**, *474*(7349), 54-60.
[128] Jelinkova, I.; Yan, Z.; Liang, Z.; Moonat, S.; Teisinger, J.; Stojilkovic, S.S.; Zemkova, H. Identification of P2X4 receptor-specific residues contributing to the ivermectin effects on channel deactivation. *Biochem. Biophys. Res. Commun.,* **2006**, *349*(2), 619-625.
[129] Silberberg, S.D.; Li, M.; Swartz, K.J. Ivermectin Interaction with transmembrane helices reveals widespread rearrangements during opening of P2X receptor channels. *Neuron,* **2007**, *54*(2), 263-274.
[130] Norenberg, W.; Sobottka, H.; Hempel, C.; Plotz, T.; Fischer, W.; Schmalzing, G.; Schaefer, M. Positive allosteric modulation by ivermectin of human but not murine P2X7 receptors. *Br. J. Pharmacol.,* **2012**, *167*(1), 48-66.
[131] Faria, R.X.; Defarias, F.P.; Alves, L.A. Are second messengers crucial for opening the pore associated with P2X7 receptor? *Am. J. Physiol. Cell. Physiol.,* **2005**, *288*(2), C260-271.
[132] Gu, B.J.; Saunders, B.M.; Jursik, C.; Wiley, J.S. The P2X7-nonmuscle myosin membrane complex regulates phagocytosis of nonopsonized particles and bacteria by a pathway attenuated by extracellular ATP. *Blood,* **2010**, *115*(8), 1621-1631.
[133] Igawa, T.; Higashi, S.; Abe, Y.; Ohkuri, T.; Tanaka, H.; Morimoto, S.; Yamashita, T.; Tsuda, M.; Inoue, K.; Ueda, T. Preparation and characterization of a monoclonal antibody against the refolded and functional extracellular domain of rat P2X4 receptor. *J. Biochem.,* **2013**, *153(*3), 275-282.
[134] Kim, M.; Yoo, O.J.; Choe, S. Molecular assembly of the extracellular domain of P2X2, an ATP-gated ion channel. *Biochem. Biophys. Res. Commun.,* **1997**, *240*, (3), 618-622.
[135] Singh, H.; Warburton, S.; Vondriska, T.M.; Khakh, B.S. Proteomics to identify proteins interacting with P2X2 ligand-gated cation channels. *J. Vis. Exp.,* **2009**, (27).
[136] Eifler, N.; Duckely, M.; Sumanovski, L.T.; Egan, T.M.; Oksche, A.; Konopka, J.B.; Luthi, A.; Engel, A.; Werten, P.J. Functional expression of mammalian receptors and membrane channels in different cells. *J. Struct. Biol.,* **2007**, *159*(2), 179-193.
[137] Reeves, P.J.; Callewaert, N.; Contreras, R.; Khorana, H.G. Structure and function in rhodopsin: high-level expression of rhodopsin with restricted and homogeneous N-glycosylation by a tetracycline-inducible N-acetylglucosaminyltransferase I-negative HEK293S stable mammalian cell line. *Proc. Natl. Acad. Sci. USA,* **2002**, *99*(21), 13419-13424.

FIGURE LEGENDS

Figure 1. Representations of the crystal structures of zfP2X4.1. The *apo*-zfP2X4-B2 (PDB ID 4DW0) crystal structure viewed from the side (A) and the top (extracellular side) (C). The ATP bound zfP2X4-C (PDB ID 4DW1) crystal structure viewed from the side (B) and the top (extracellular side) (D). Each subunit is represented by a different colour. ATP in the binding pocket between 2 adjacent subunits is shown in cyan.

Figure 2. The ATP binding site of P2X receptors. (A) ATP-binding site of zfP2X4.1 (PDB ID 4DW1) (B) ATP binding site in a molecular model of rP2X2. Black dashed lines designate hydrogen bonds. ATP is shown in orange and blue with nitrogen and oxygen atoms represented in dark blue and red respectively. Residues from chain A are shown in green. Residues from chain B are shown in grey.

Figure 3. Schematic of a zfP2X4.1 monomer and location of disulphide bonds. (A) Schematic structure of a zfP2X4.1 monomer, showing the analogy of the receptor monomer to a dolphin with labelled domains. (B) Close-up of the head domain showing the location of the disulphide bond pairs 1-6, 2-4 and 3-5 (yellow). (C) Close-up of the body and dorsal fin domains showing the location of the disulphide bond pairs 7-8 and 9-10 (yellow).

Figure 4. Comparison of zfP2X4.1 with ASIC1. (A) Side view of the zfP2X4.1 structure in the ATP-bound, open conformation. (PDB ID 4DW1). (B) Side view of the chicken ASIC1 structure in the psalmotoxin-bound, open conformation (PDB ID 4FZ0). (C) Top view of the zfP2X4.1 TM helices in the open state (PDB ID 4DW1). (D) Top view of the chicken ASIC1 TM helices in the closed state (PDB ID 3IJ4).

Figure 5. Comparison of low-resolution P2X receptor structures derived from TEM and single particle analysis. (A) Cryo-EM structure of rP2X2 (adapted from [76] with permission. (B) Negative-stain TEM structure of hP2X4, displayed at two volume thresholds (the inner threshold is consistent with the mass of a P2X4 trimer plus detergent micelle; adapted from [77]). (C) Negative-stain TEM structure of DdP2XA (black mesh) fitted with the crystal structure of zfP2X4.1 (green cartoon; PDB 3H9V; adapted from [57]). (D) Negative-stain TEM structure of hP2X1 in the absence of ATP; the head region of the receptor is indicated (adapted from [14]). (E) Negative-stain TEM of hP2X1 in the presence of 1 mM ATP (blue volume; overlayed with the native state (black mesh) for comparison; the appearance of a lateral portal just above the TM region is indicated (adapted from [14]). Each panel is a side-view and is represented at approximately the same scale as panel (A). The approximate position of the TM region is indicated by solid blue lines in (A) and dashed black lines in (C), (D) and (E).

Supplementary Figure 1. Sequence alignment of selected mammalian P2X receptors with zfP2X4.1
The start and the end of the zfP2X4.1 sequence present in the crystal structure (PDB ID 3H9V) are indicated with red arrows. The percentage amino-acid identities (between the full-length receptors) are indicated by the numbers in brackets next to the sequence names at the start of the alignment. TM1 and TM2 are indicated by green and blue double-headed arrows respectively. The ten conserved cysteine residues in the extracellular domain are indicated in green, the amino-acids which contribute to the ATP binding site are indicated in yellow, the amino-acids contributing to the channel pore are indicated in cyan, and the conserved lysine which contributes to both ATP binding and channel gating is indicated in red. The long C-terminal domains of P2X2 and P2X7, for which there is no structural information, are omitted.

FIGURE 1

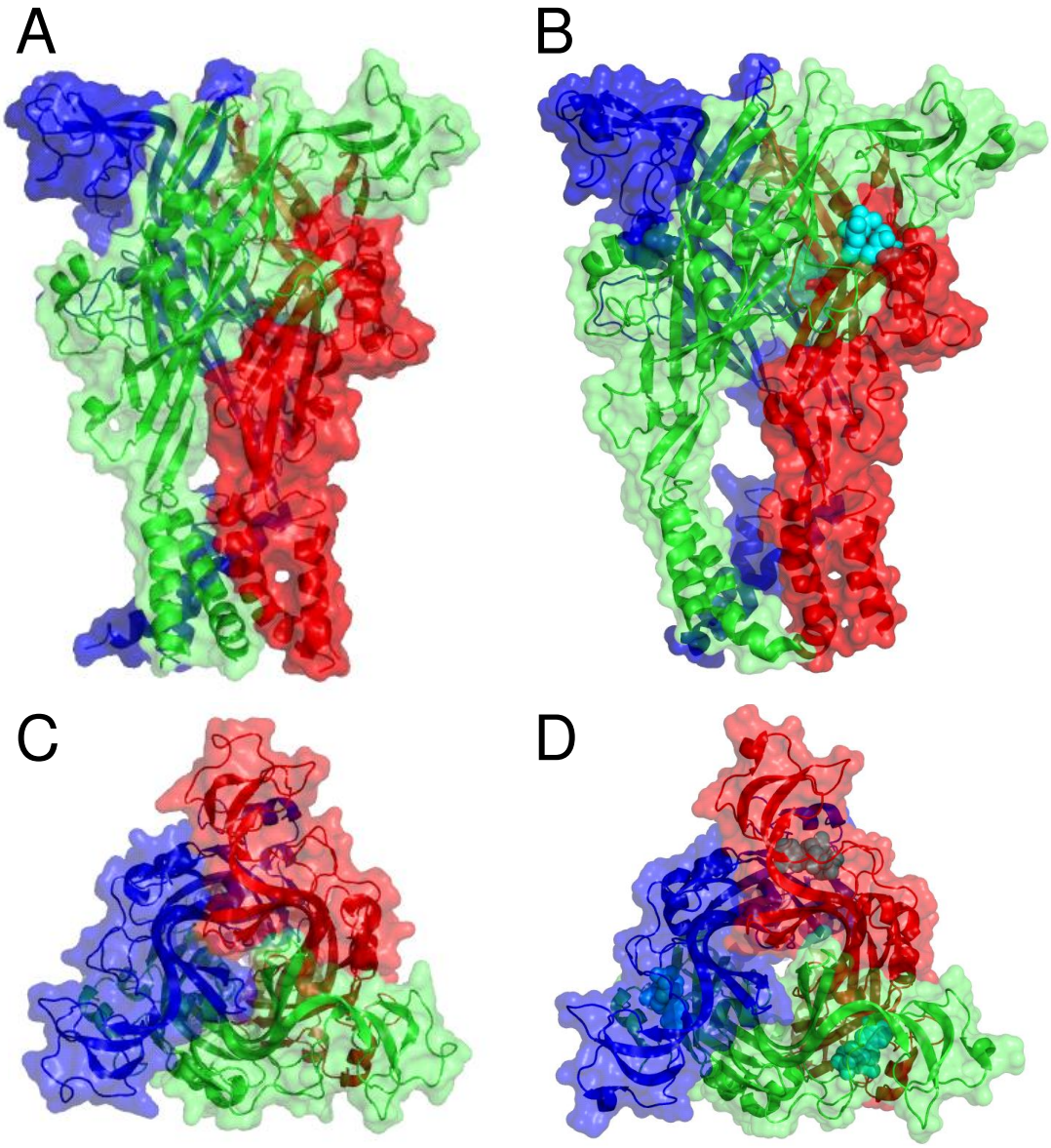

FIGURE 2

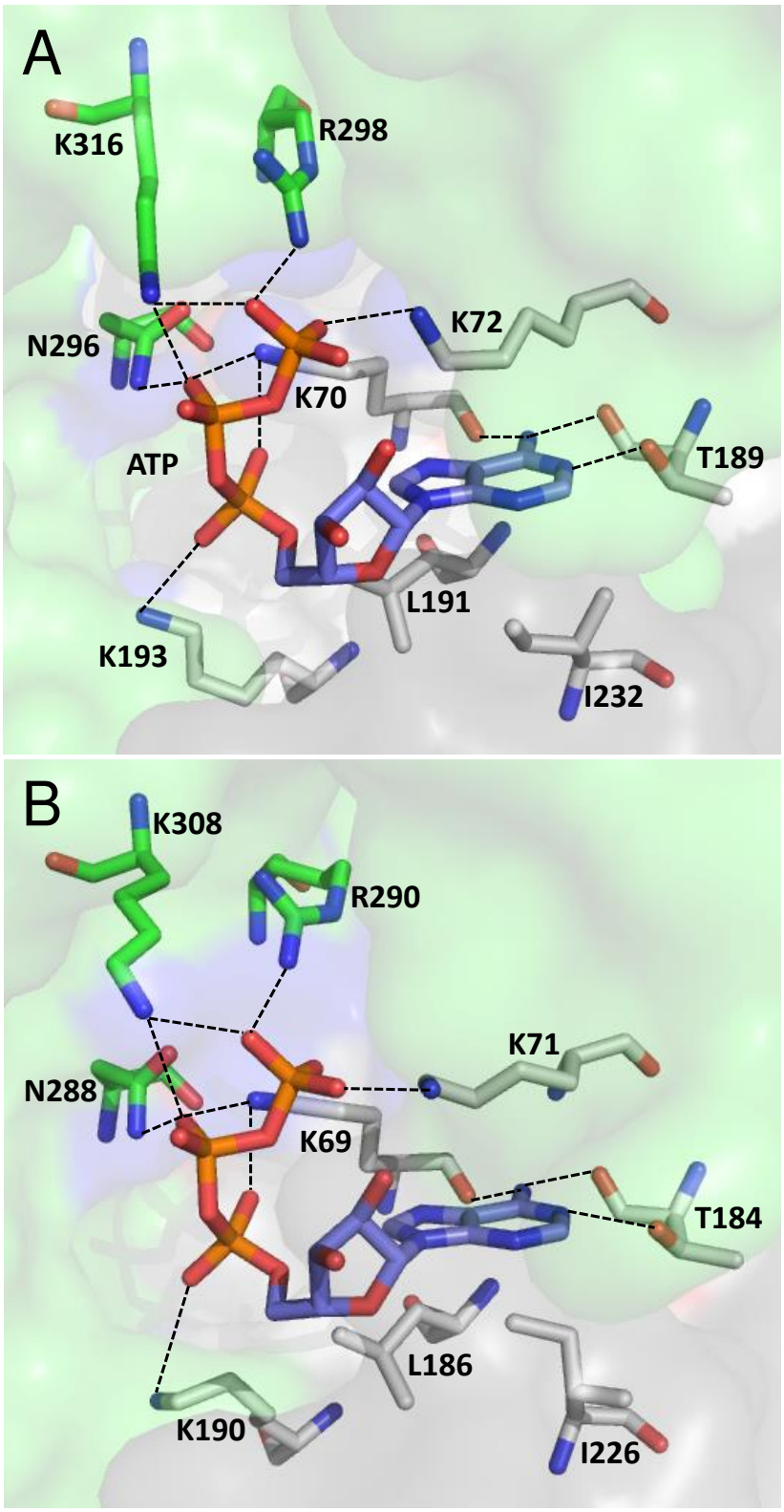
A
K316
R298
N296
K72
K70
ATP
T189
L191
K193
I232
B
K308
R290
K71
N288
K69
T184
L186
K190
I226

FIGURE 3

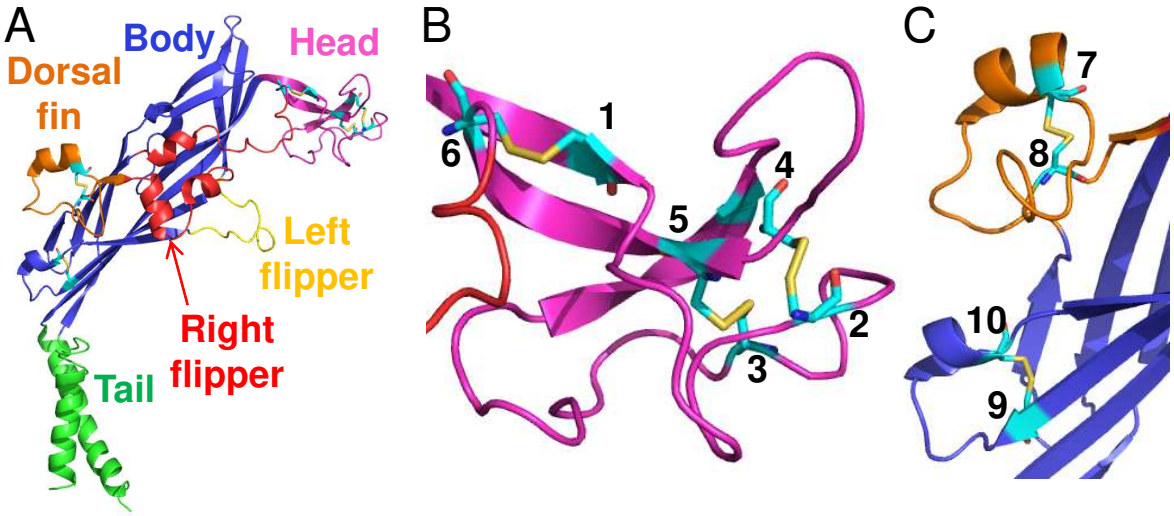
A
Body
Head
Dorsal fin
Left flipper
Right flipper
Tail
B
1
6
4
5
2
3
C
7
8
10
9

FIGURE 4

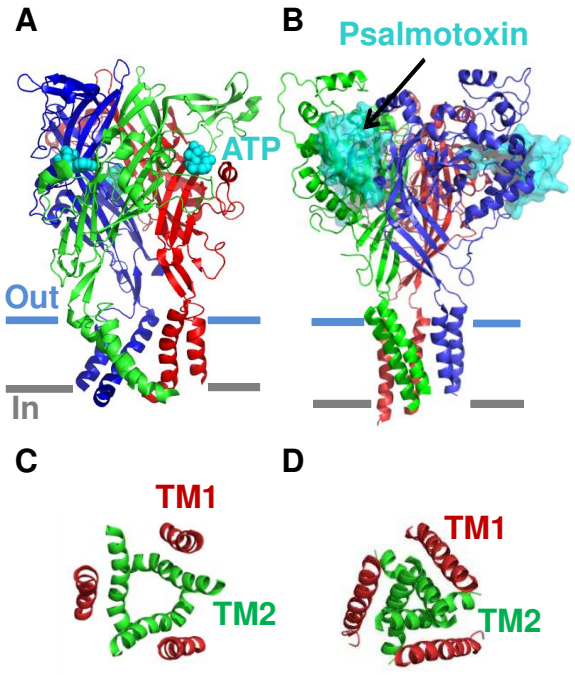

FIGURE 5

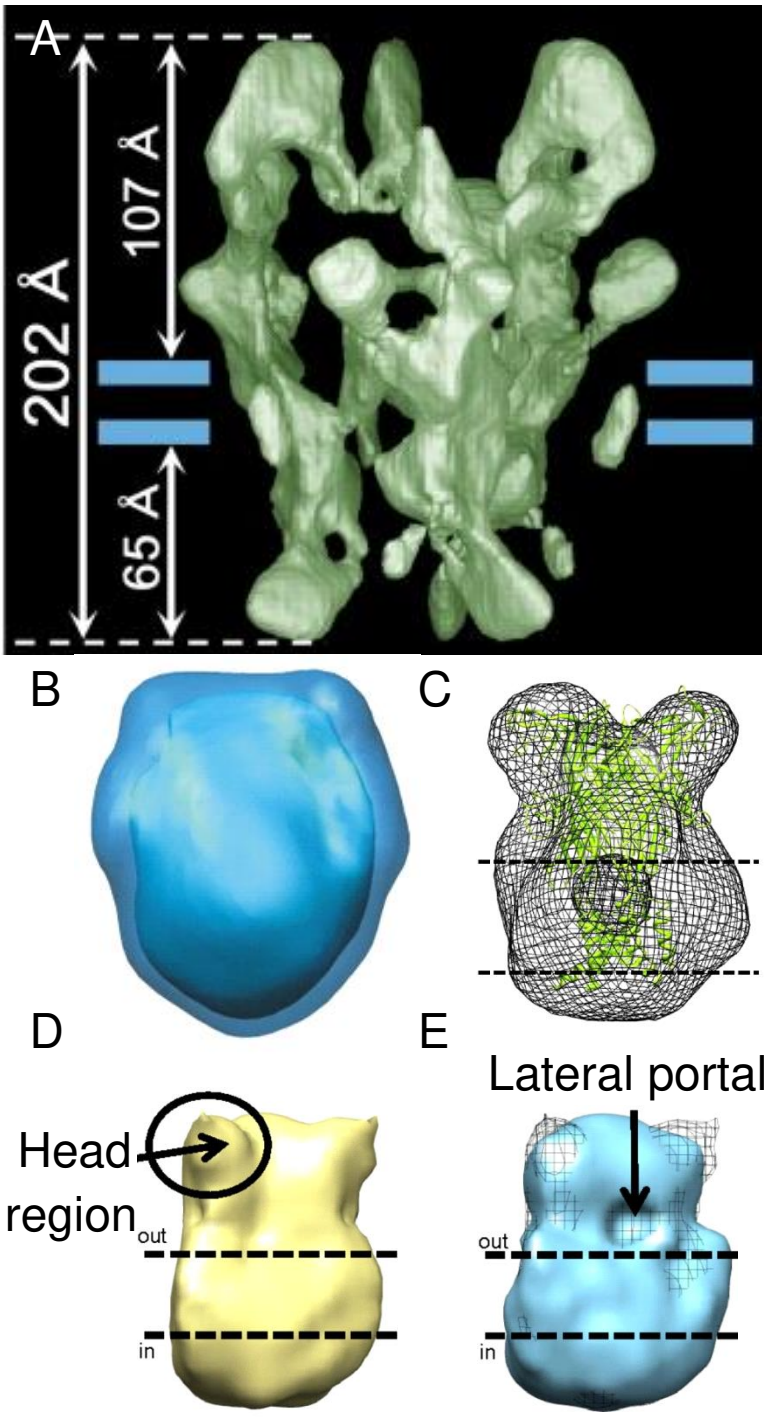

Supplementary Figure 1

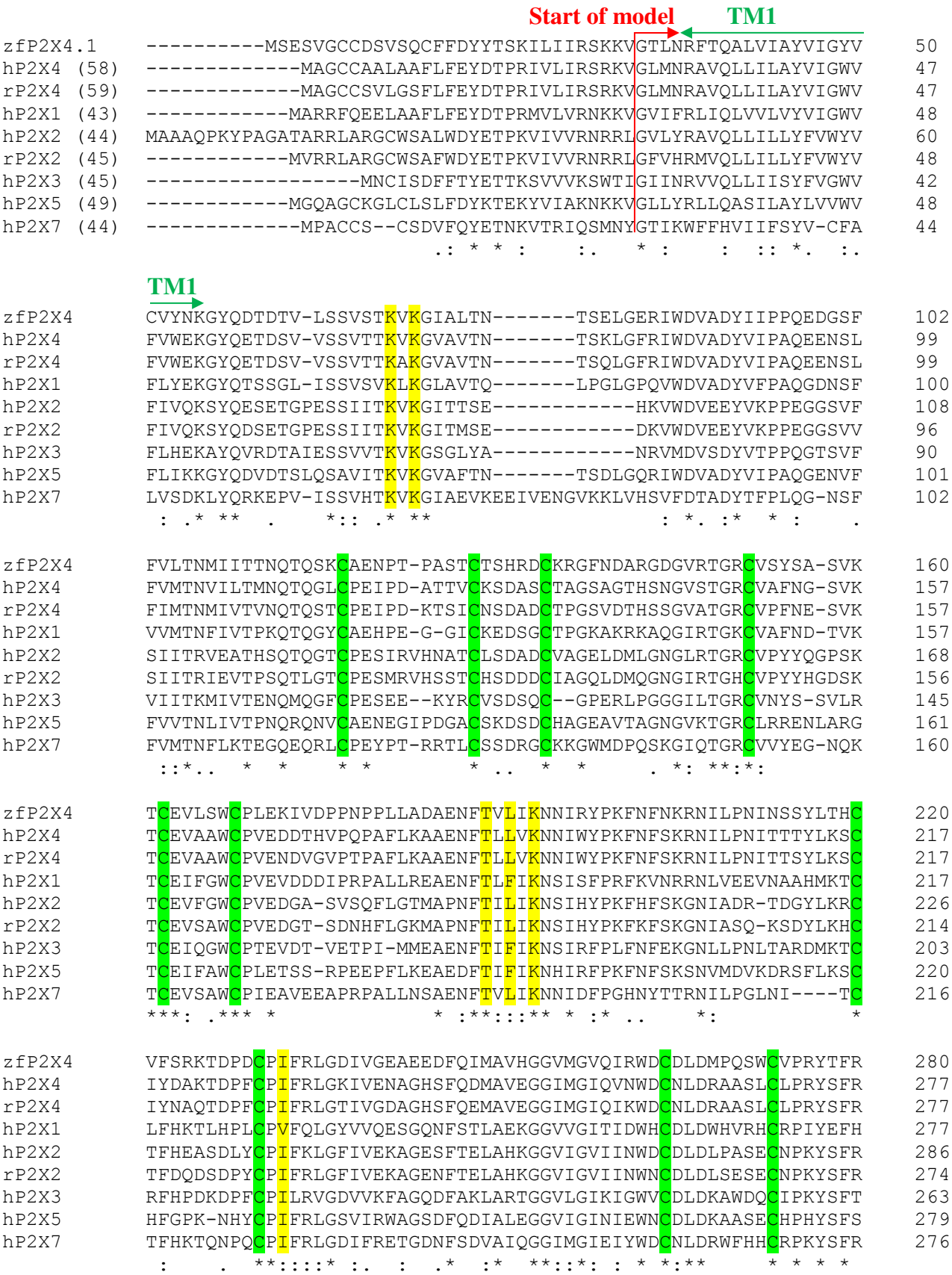

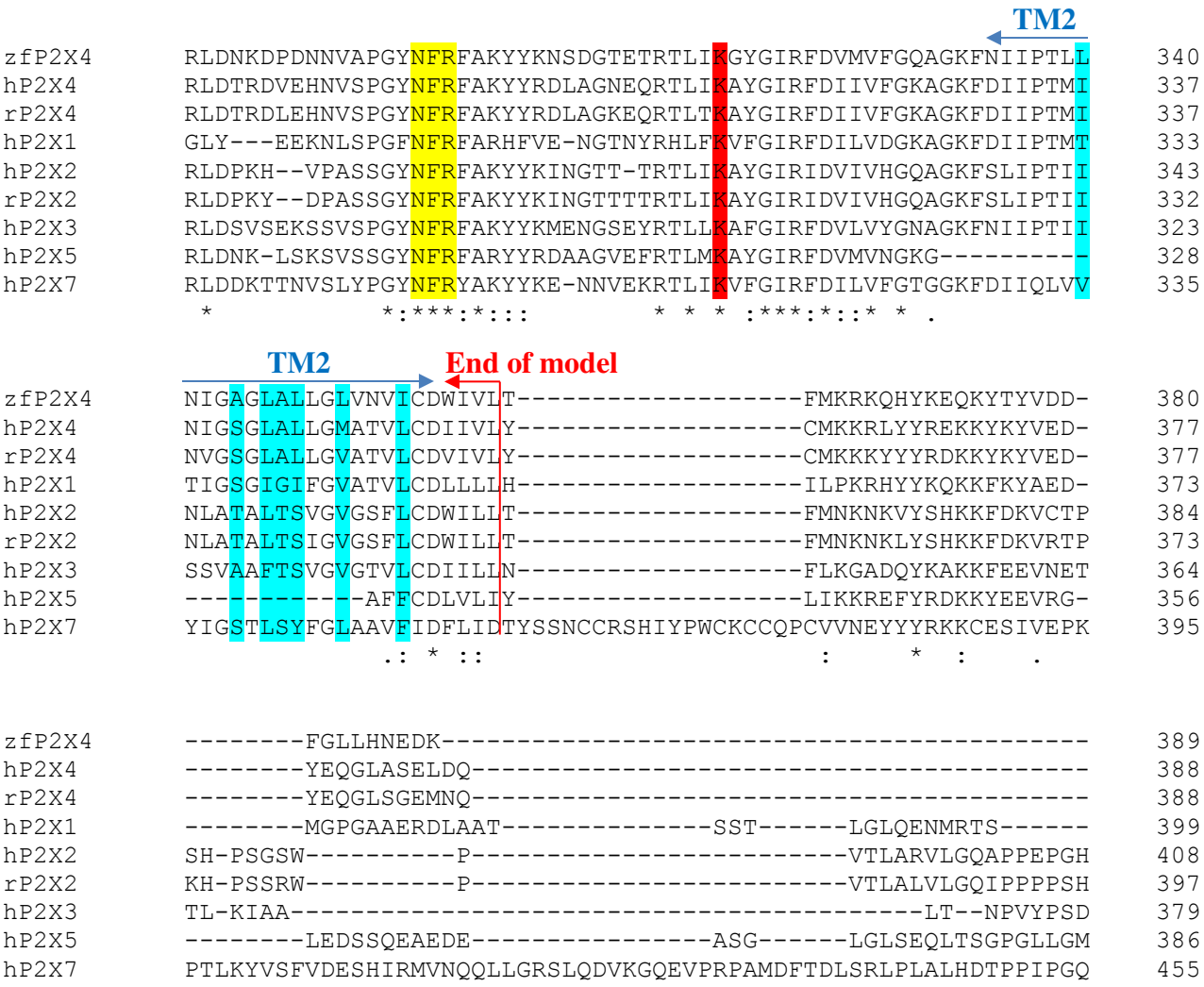


```
                                                                                                  TM2
zfP2X4      RLDNKDPDNNVAPGYNFRFAKYYKNSDGTETRTLIKGYGIRFDVMVFGQAGKFNIIPTLL     340
hP2X4       RLDTRDVEHNVSPGYNFRFAKYYRDLAGNEQRTLIKAYGIRFDIIVFGKAGKFDIIPTMI     337
rP2X4       RLDTRDLEHNVSPGYNFRFAKYYRDLAGKEQRTLTKAYGIRFDIIVFGKAGKFDIIPTMI     337
hP2X1       GLY---EEKNLSPGFNFRFARHFVE-NGTNYRHLFKVFGIRFDILVDGKAGKFDIIPTMT     333
hP2X2       RLDPKH--VPASSGYNFRFAKYYKINGTT-TRTLIKAYGIRIDVIVHGQAGKFSLIPTII     343
rP2X2       RLDPKY--DPASSGYNFRFAKYYKINGTTTTRTLIKAYGIRIDVIVHGQAGKFSLIPTII     332
hP2X3       RLDSVSEKSSVSPGYNFRFAKYYKMENGSEYRTLLKAFGIRFDVLVYGNAGKFNIIPTII     323
hP2X5       RLDNK-LSKSVSSGYNFRFARYYRDAAGVEFRTLMKAYGIRFDVMVNGKG----------     328
hP2X7       RLDDKTTNVSLYPGYNFRYAKYYKE-NNVEKRTLIKVFGIRFDILVFGTGGKFDIIQLVV     335
             *           *:***:*:::        * * * :***:*::* * .

                  TM2          End of model
zfP2X4      NIGAGLALLGLVNVICDWIVLT-------------------FMKRKQHYKEQKYTYVDD-     380
hP2X4       NIGSGLALLGMATVLCDIIVLY-------------------CMKKRLYYREKKYKYVED-     377
rP2X4       NVGSGLALLGVATVLCDVIVLY-------------------CMKKKYYYRDKKYKYVED-     377
hP2X1       TIGSGIGIFGVATVLCDLLLLH-------------------ILPKRHYYKQKKFKYAED-     373
hP2X2       NLATALTSVGVGSFLCDWILLT-------------------FMNKNKVYSHKKFDKVCTP     384
rP2X2       NLATALTSIGVGSFLCDWILLT-------------------FMNKNKLYSHKKFDKVRTP     373
hP2X3       SSVAAFTSVGVGTVLCDIILLN-------------------FLKGADQYKAKKFEEVNET     364
hP2X5       ----------AFFCDLVLIY-------------------LIKKREFYRDKKYEEVRG-     356
hP2X7       YIGSTLSYFGLAAVFIDFLIDTYSSNCCRSHIYPWCKCCQPCVVNEYYYRKKCESIVEPK     395
                       .: * ::                       :    *  :    .

zfP2X4      --------FGLLHNEDK-----------------------------------------     389
hP2X4       --------YEQGLASELDQ-----------------------------------------     388
rP2X4       --------YEQGLSGEMNQ-----------------------------------------     388
hP2X1       --------MGPGAAERDLAAT--------------SST------LGLQENMRTS------     399
hP2X2       SH-PSGSW----------P------------------------VTLARVLGQAPPEPGH     408
rP2X2       KH-PSSRW----------P------------------------VTLALVLGQIPPPPSH     397
hP2X3       TL-KIAA-----------------------------------------LT--NPVYPSD     379
hP2X5       --------LEDSSQEAEDE----------------ASG------LGLSEQLTSGPGLLGM     386
hP2X7       PTLKYVSFVDESHIRMVNQQLLGRSLQDVKGQEVPRPAMDFTDLSRLPLALHDTPPIPGQ     455
```